Publication for the Special Issue of the Journal of Mechanical Systems and Signal Processing
"EuroMech-401, Inverse Methods in Structural Dynamics," Edited by J. E. Mottershead.
Article mssp.2000.XXXX. Vol. 14, No. XX, XXXX 2000, pp. 1-44.

REVIEW AND ASSESSMENT OF MODEL UPDATING FOR NONLINEAR, TRANSIENT DYNAMICS

François M. Hemez[1] and **Scott W. Doebling**[2]
Engineering Analysis Group (ESA-EA)
Los Alamos National Laboratory, P.O. Box 1663, M/S C926
Los Alamos, New Mexico 87545, U.S.A.

ABSTRACT

The purpose of this publication is to motivate the need of validating numerical models based on time-domain data for nonlinear, transient, structural dynamics and to discuss some of the challenges faced by this technology. Our approach is two-fold. First, several numerical and experimental testbeds are presented that span a wide variety of applications (from nonlinear vibrations to shock response) and difficulty (from a single-degree of freedom system with localized nonlinearity to a 3D, multiple-component assembly featuring nonlinear material response and contact mechanics). These testbeds have been developed at Los Alamos National Laboratory (LANL) in support of the advanced strategic computing initiative and our code validation and verification program. Conventional, modal-based updating techniques are shown to produce erroneous models although the discrepancy between test and analysis modal responses can be bridged. This conclusion offers a clear justification that metrics based on modal parameters are not well suited to the resolution of inverse, nonlinear problems. In the second part of this work, the state-of-the-art in the area of model updating for nonlinear, transient dynamics is reviewed. The techniques identified as the most promising are assessed using data from our numerical or experimental testbeds. Several difficulties of formulating and solving inverse problems for nonlinear dynamics are identified. Among them, we cite the formulation of adequate metrics based on time series and the need to propagate variability throughout the optimization of the model's parameters. Another important issue is the necessity to satisfy continuity of the response when several finite element optimizations are successively carried out. The publication concludes with a brief description of the framework developed at LANL for the probabilistic validation and verification of nonlinear structural models. This discussion is illustrated with results obtained when parameters of a model are optimized such that acceleration signals become statistically consistent with measurements obtained during a series of impact tests.

[1] Technical Staff Member, ESA-EA, hemez@lanl.gov, 505-665-7955 (Voice), 505-665-2137 (Fax).

[2] Technical Staff Member, ESA-EA, doebling@lanl.gov, 505-667-6950 (Voice), 505-665-2137 (Fax).

NOMENCLATURE

The "Standard Notation for Modal Testing & Analysis" is used throughout this paper, see Reference [1]. Symbols not commonly used in the modal testing and structural dynamics communities are defined in the text.

1. INTRODUCTION

Inverse problem solving is at the core of engineering practices as such work generally involves designing a system to target a given performance or to satisfy operating constraints. Increasingly, designers are faced with shorter design cycles while their testing capabilities are reduced and the physics they must understand becomes more sophisticated. The consequence is the need for larger-size computer models, coupled-field calculations and more accurate representations of the physics. To improve the predictive quality of numerical models and enhance the capability to extrapolate the response of a system, it is often necessary to formulate and solve inverse problems where simulations are compared to field measurements [2]. In addition, it has been recognized that non-deterministic approaches must be employed to alleviate our lack of test data and incomplete understanding of mechanics [3].

The work presented in this publication deals with the formulation of inverse problems for correlating transient dynamics to responses obtained from nonlinear finite element models. The application targeted is clearly structural dynamics although most of the techniques discussed here either originate or find their counterparts in physics and other engineering fields. The reason why time series rather than modal parameters are considered is essentially because the increasing complexity and sophistication of engineering applications makes it necessary to analyze systems with arbitrary sources of nonlinearity. Another motivation is the modeling of transient dynamic events, such as explosive or shock responses, for which modal solutions make no sense due to the clustering of high-frequency modes. For clarity, this paper is organized according to three main parts. First, several numerical and experimental testbeds are presented. These are used later for generating reference data or test data that feeds various test-analysis reconciliation techniques. Our intent is to introduce a series of problems that feature various sources of nonlinearity and modeling difficulties and that can be used to challenge the existing model updating strategies. The second part reviews the state-of-the-art in model updating and error control algorithms. The performance of several such techniques is assessed with data generated or collected using our testbeds. This demonstration is not an exhaustive assessment of each method's advantages and limitations. The objective is rather to identify and resolve the critical deficiencies with the ultimate goal of applying this technology to the problem of assessing the quality of a nonlinear numerical model. Finally, a discussion follows that presents some of the key aspects that, we believe, will drive the development of test-analysis correlation and model validation technology in the years to come.

Among the applications of interest, we cite the development of numerical models for nonlinear vibration problems. This would be the situation encountered when a mostly linear system is connected to a secondary component. A good example is the dynamics of a delivery vehicle-payload assembly. At the interface between the two, several sources of nonlinearity and various energy dissipation mechanisms may have to be incorporated into the model. One of our experimental testbeds is geared towards the modeling and analysis on nonlinear vibrating systems. The other one features the impact of a steel cylinder that compresses a layer of elastomeric material otherwise difficult to characterize with conventional testing procedures [4]. By correlating the transient acceleration response to field measurements, this behavior is characterized and high-fidelity, physics-based modeling of the material can be optimized. In the effort to reproduce the test data, several models are developed by varying, among other things, the constitutive law and the type of modeling. Then, the problem consists of assessing the degree of correlation between test and analysis data and to carry out parametric optimization in an effort to validate each candidate model.

The publication is organized as follows. Section 2 offers a description of the four testbeds developed for validating the existing model updating technology. We emphasize that the focus of this work is the development of model validation strategies for nonlinear dynamics and/or highly transient events. Our testbeds reflect this preoccupation. Section 3 summarizes conclusions reached after applying some of the available test-analysis correlation techniques to nonlinear vibrating systems. The illustration presented in Section 3 features a 8-degree of freedom, mass-spring system. Nonlinearity is introduced by the joint means of friction and a contact/impact mechanism. In addition to showing the limitations posed by conventional, modal-based techniques, time-domain methods are tested for their ability to identify damage in one of the linear springs. Section 4 draws on the previous conclusions by showing that optimal control strategies must be used for addressing the main drawback of time-domain formulations, that is, their inability to enforce continuous solution fields. Unfortunately, this additional constraint introduces a two-point boundary value problem, the resolution of which at each step of the optimization is not (yet) compatible with the analysis of large-size, structural models. Finally, Section 5 proposes a general discussion of model validation applied to nonlinear systems and transient test data. Among other issues, we emphasize the three key aspects of 1) enabling probabilistic structural analysis; 2) providing an efficient characterization of the data by extracting multiple "features;" and 3) integrating statistical tests to the definition of the cost function for parametric optimization.

2. TESTBEDS FOR THE VALIDATION OF NONLINEAR STRUCTURAL MODELS

In this Section, several numerical and experimental testbeds are presented. They have been found in the literature or developed in support of the advanced strategic computing initiative and our code validation and verification program. The examples discussed span a wide variety of applications and difficulty. The first three (Sections 2.1 and 2.2) involve nonlinear vibrating systems. The last one (Section 2.3) represents a high-frequency, transient shock response. The sources of nonlinearity considered are either purely analytical (cubic springs are used throughout Section 2.1), undetermined but localized (impact mechanism in Section 2.2) or parametric and distributed (hyperfoam material and contact dynamics in Section 2.3). These examples also feature various mechanisms for the dissipation of energy that can not, we believe, be reduced to the conventional, modal representation of damping.

2.1. NUMERICAL TESTBEDS WITH A CUBIC NONLINEARITY

The first two testbeds discussed are purely analytical. They are formed of masses and linear springs. Damping is considered in the first case only. The first system exhibits a single degree of freedom and the second system has four degrees of freedom. In both cases, the source of nonlinearity considered is a cubic spring, that is, the nonlinear, internal force is proportional to the third power of a displacement. The advantage of these numerical simulators is that the modeling error and the noise-to-signal ratio can be controlled explicitly.

2.1.1. *Single Degree of Freedom Oscillator*

Our first numerical testbed is the single degree of freedom system pictured in Figure 1. This system is also known as the Duffing oscillator and it has been studied extensively for the ability of its response $x(t)$ to transition from ordered to chaotic behavior. The equation of motion, the harmonic forcing function considered here and the nonlinear, internal force are defined in equation (1). In the numerical tests performed, reference data are generated by integrating equation (1) over a period of 30 sec. Then, the internal force is removed to introduce a modeling error. The purpose of test-analysis correlation is therefore to identify this missing term.

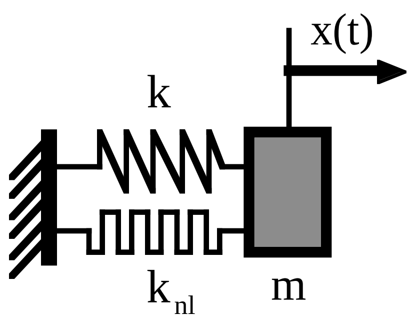

$$
\begin{gathered}
m \frac{\partial^2 x}{\partial t^2}(t) + d \frac{\partial x}{\partial t}(t) + kx(t) + F_{int}(t) = F_{ext}(t) \\
F_{ext}(t) = F_o \cos(\Omega t); F_{int}(t) = k_{nl} x^3(t) \\
m = 2.56; d = 0.32; k = 1; k_{nl} = 0.05; F_o = 2.5; \Omega = 1
\end{gathered}
\tag{1}
$$

Figure 1. Numerical testbed: single degree of freedom mass/spring system with cubic nonlinearity.

Simulated “measurements” are assumed to be available only at eleven equally-spaces samples. These consist of displacement and velocity data. A total of 75 time increments are typically used to integrate the equation of motion in time between any two measurements. Although this testbed is probably the simplest one that could be imagined, the amount of computation required for solving the inverse problem may be enormous (see Section 4). Figure 2 shows the difference between test and analysis time-histories before the model is optimized. Displacements are shown on the top half and velocities are shown on the bottom half. Clearly, the response predicted by the linear model is inconsistent with test data. It is emphasized that measurements are assumed available only at the eleven samples symbolized by the stars in Figure 2.

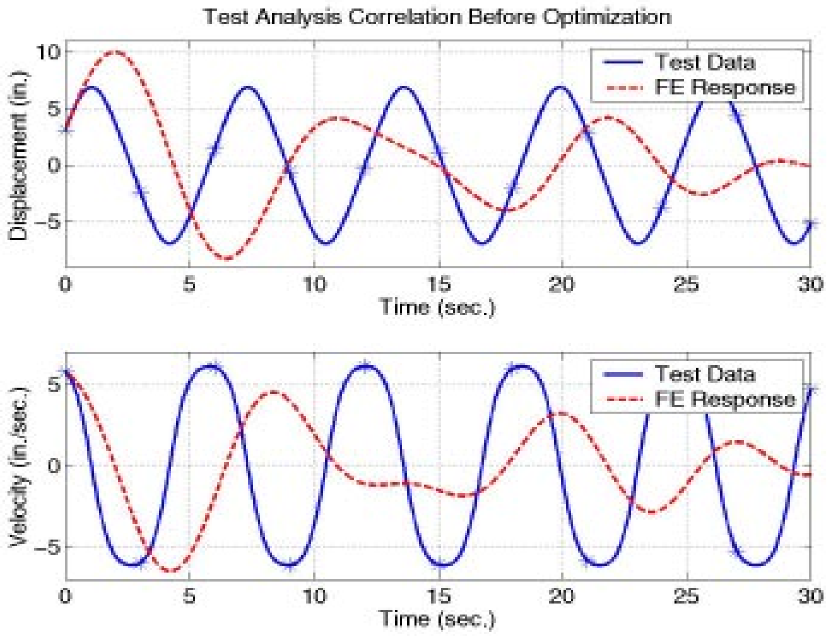

Figure 2. Test-analysis correlation of the single degree of freedom system before model updating. (Top half, displacement time-history; Bottom half, velocity time-history.)

2.1.2. *Multiple-Degree of Freedom Oscillator*

The second system investigated is a 4-degree of freedom, mass/spring system with cubic nonlinearity. Figure 3 provides an illustration and the nonlinear, internal force added to the equation of motion is defined in equation (2). This system generalizes the Duffing oscillator to a multiple-degree of freedom case. A higher dimensionality is required to study the effect of spatial incompleteness, that is, the effect of measuring the response at a subset of the model's degrees of freedom. The system shown in Figure 3 is excited with a random excitation and numerical integration is used for obtaining the time-history of acceleration, velocity and displacement at the four degrees of freedom. A total of 0.2 sec. worth of data are generated with a sampling period of 1.0e-04 sec. The reference data consist of 200 equally-spaced "measurements" at locations 1, 3 and 4. The objective of this test is to recover a 15% stiffness reduction of the third linear spring when one of the system's output is not available.

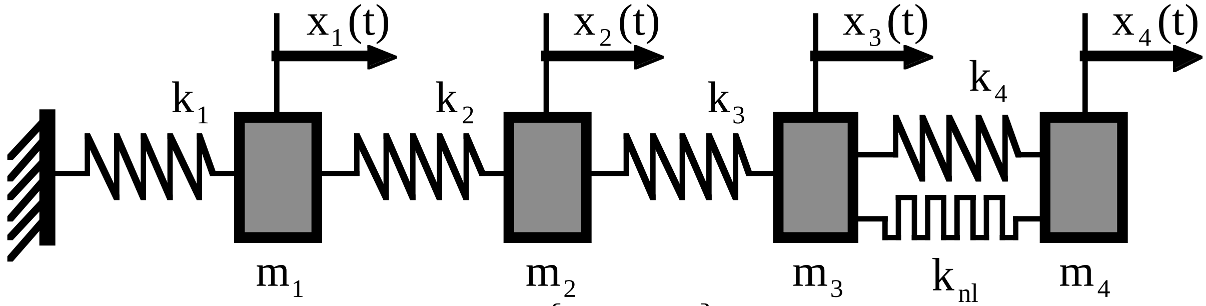

$$\{F_{int}(t)\} = \begin{Bmatrix} 0 \\ 0 \\ 0 \\ k_{nl}\left(x_4(t)\right)^3 \end{Bmatrix} \tag{2}$$

Figure 3. Numerical testbed: 4-degree of freedom mass/spring system with cubic nonlinearity. (Damage is induced at spring number 3 and measurements are assumed available at locations 1, 3 and 4.)

2.2. EXPERIMENTAL TESTBED FOR NONLINEAR VIBRATIONS

Our testbed for model validation in the context of nonlinear vibration is the LANL 8-DOF (which stands for Los Alamos National Laboratory eight degrees of freedom) system illustrated in Figure 4. It consists of eight masses connected by linear springs. The masses are free to slide along a center rod that provides support for the whole system. It also introduces a significant source of friction that constitutes the first modeling challenge.

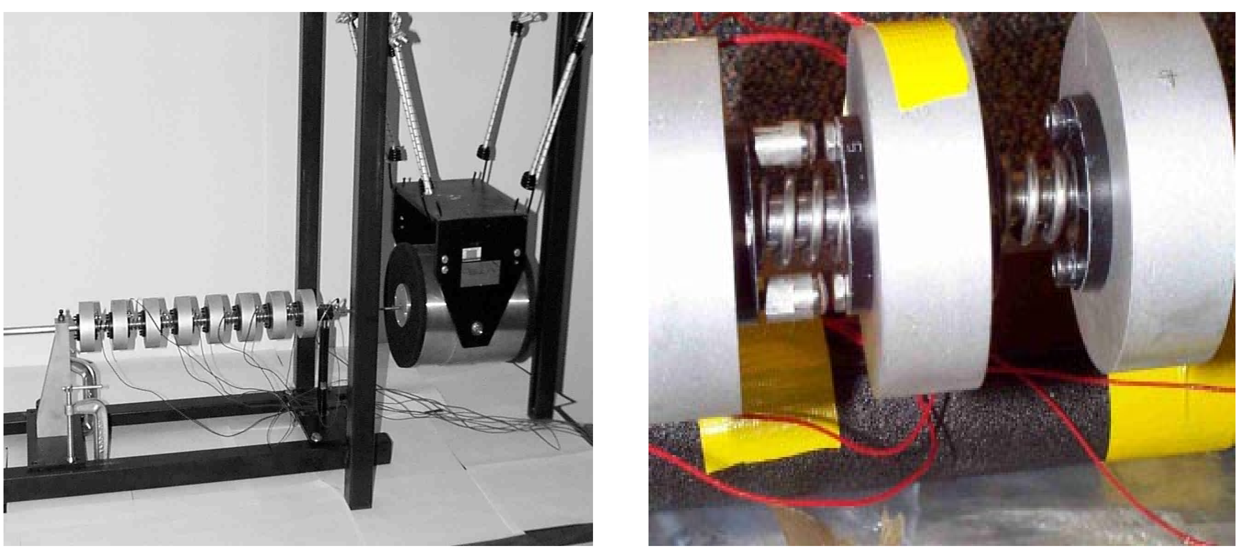

Figure 4. LANL 8-DOF testbed. (Left: illustration of the system of its support stand. Right: contact mechanism between masses 5 and 6.)

Vibration tests are performed on the nominal system and on a damaged version where the stiffness of one of the springs is reduced by 14%. The excitation is applied at the first degree of freedom (which therefore defines a driving point measurement) and it consists of a random signal at various force amplitudes. Data generated via impulse testing (hammer excitation) are also available. The response is collected over a period of eight seconds with a total of 2^{13} = 8,192 samples. A contact mechanism can be added between two masses to induce a source of contact/impact, see Figure 4. This is achieved by attaching to two neighboring masses a pair of short, rigid rods with a very small clearance between their extremities. As the system vibrates and the contact rods "bump" into each other, the dynamics becomes increasingly nonlinear. Analyzing the test data using time-frequency tools such as wavelet transforms shows significant shifts of the frequency content, making it somewhat difficult to rely on linear, resonant modes to characterize this system.

Time-domain acceleration data are measured at each one of the eight masses and modal parameters are identified using a classical frequency-domain curve fitting algorithm. Table 1 shows that the original, linear and undamped model is in good agreement with the identified modal parameters prior to any parametric adjustment. Nevertheless, an optimization is performed to resolve the more-or-less uniform shift in frequency seen in Table 1 for the first three modes. The test discussed in this publication consists of identifying the damaged spring using a linear model that does not account for the friction nor the source of contact/impact. The performance of conventional model updating approaches is evaluated when the distance between test data and modeling is defined using modal parameters (resonant frequencies and mode shapes). Time-domain techniques are also tested in Section 3 for their ability to identify the (unknown) nonlinearity when less measurements than degrees of freedom are available.

Table 1. Test-analysis correlation of the LANL 8-DOF testbed for nonlinear vibrations. (The table shows the correlation between the nominal, undamaged system without impact between the masses and the corresponding linear model.)

Mode Number	Identified Frequency	FE Model Frequency	Modal Assurance Criterion (MAC)	Frequency Error
1	22.3 Hz	21.8 Hz	99.7%	-2.3%
2	43.9 Hz	43.0 Hz	99.4%	-2.0%
3	64.8 Hz	63.0 Hz	99.4%	-2.8%
4	85.9 Hz	80.8 Hz	93.2%	-6.0%
5	99.7 Hz	95.6 Hz	98.5%	-4.1%

Finally, we mention that test data from the 8-DOF LANL testbed can be made available to test model validation strategies. We believe that this is an interesting testbed because small-dimension, linear models can be developed that provide a good starting point for test-analysis correlation. Nevertheless, some of the configurations tested allow to discriminate between numerical techniques that would perform well when the dynamics remains linear but that fail when nonlinear effects dominate the response.

2.3. IMPACT TEST EXPERIMENT

The last testbed presented deals with transient responses rather than nonlinear vibrations. The application targeted is a high-frequency shock test that features a component characterized by a nonlinear, visco-elastic material behavior. Results of several explicit finite element (FE) simulations are compared to measurements and parameters of the FE models are optimized to improve the correlation.

An illustration of this setup is provided in Figure 5. It can be observed that the main two components (steel impactor and foam layer) are assembled to the carriage in a rather straightforward manner. The center of the steel cylinder is hollow and has been fixed with a rigid collar to restrict the motion of the impactor to the vertical direction. This assures perfectly bilinear contact between the steel and foam components, allowing the structure to be modeled axi-symmetrically. In spite of this, a full three-dimensional model is also developed to verify this assumption’s validity. Besides the material modeling, another important parameter in this study is the amount of preload applied by the bolt used to hold the assembly together. The torque applied was not measured during testing and it is very likely that it may have varied from test to test.

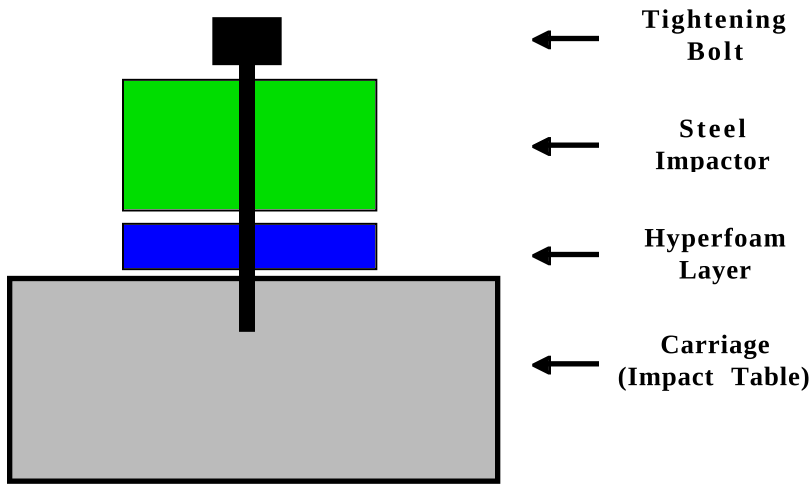

Figure 5. Description of the assembly of the cylindrical impactor and carriage.

The analysis program used for these calculations is HKS/Abaqus-Explicit, a general-purpose package for finite element modeling of nonlinear structural dynamics [5]. It features an explicit time integration algorithm, which is convenient when dealing with nonlinear material behavior, potential sources of impact or contact, and high frequency excitations. In an effort to match the test data, several FE models are developed by varying, among other things, the constitutive law and the type of modeling. Therefore, optimization variables consist of the usual design variables augmented with structural form parameters such as kinematic assumptions, geometry description (2D or 3D), contact modeling and numerical viscosity. Figure 6 illustrates two discretized models used for numerical simulations. One aspect of this experiment that we wish to emphasize is that modeling was performed prior to testing. It allowed some degree of experimental design by providing valuable insight regarding the response of the system, the type of instrumentation to be used and its configuration.

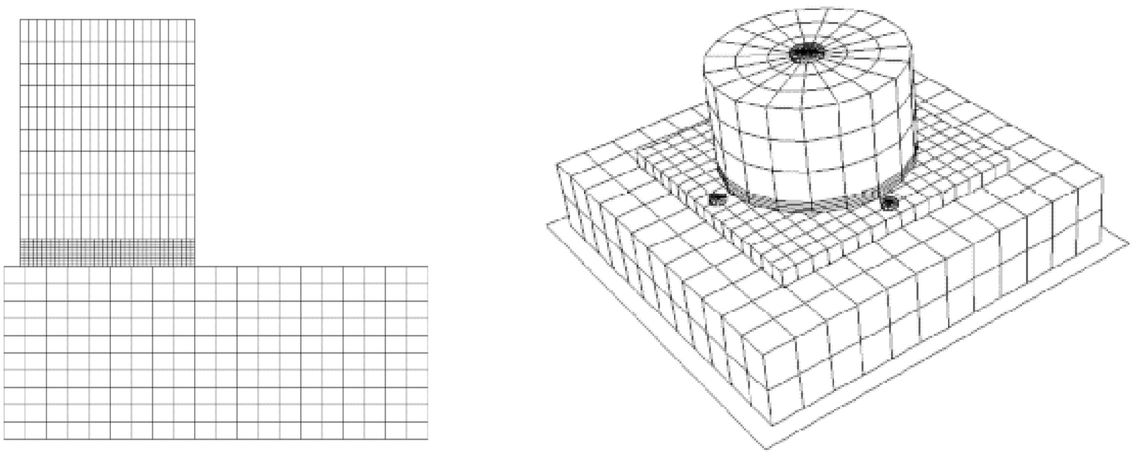

Figure 6. Axi-symmetric model (left) and 3D model (right) of the LANL impact testbed.

During the actual test, the carriage that weights 955 lbm (433 kg) is dropped from various heights and impacts a rigid floor. The input acceleration is measured on the top surface of the carriage and three output accelerations are measured on top of the steel impactor that weights 24 lbm (11 kg). Figure 7 provides an illustration of this setup.

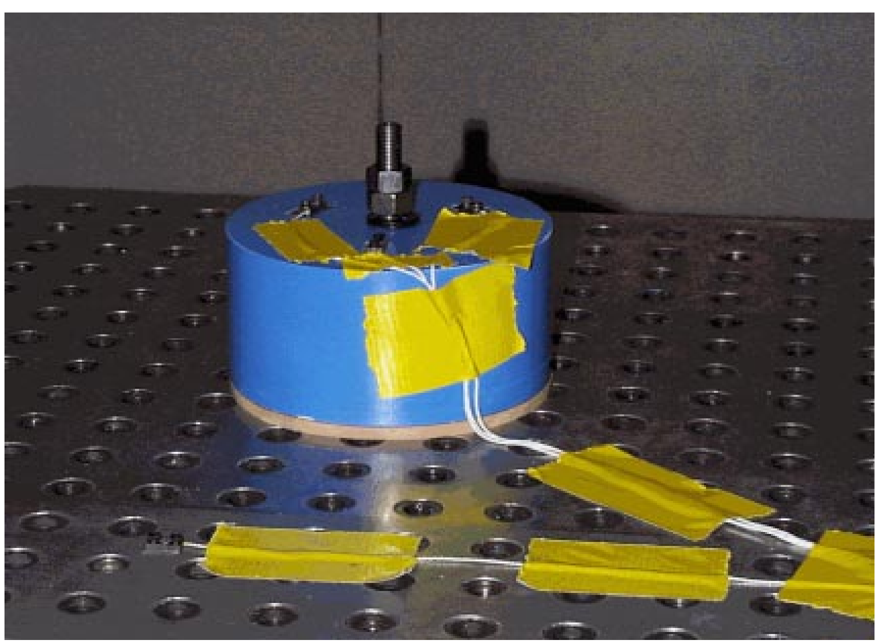

Figure 7. LANL impact test setup.

The impact test is repeated several times to collect multiple data sets from which the repeatability of the experiment can be assessed. Upon impact, the steel cylinder compresses the foam to cause elastic and plastic strains during a few μ-seconds. Typical accelerations measured during the impact tests are depicted in Figure 8. Both data sets are generated by dropping the carriage from an initial height of 13 inches (0.33 meters). Figure 8 shows on the left the acceleration response when a 1/4 inch-thick (6.3 mm) layer of foam is used and it shows on the right the acceleration response with a 1/2 inch-thick layer (12.6 mm). It can be seen that over a thousand g's are measured on top of the impact cylinder which yields large deformations in the foam layer. The time scale also indicates that the associated strain rates are important. Lastly, the variation in peak acceleration observed on Figure 8 suggests that a non-zero angle of impact is involved, making it necessary to model this system with a 3D discretization. Clearly, modal superposition techniques would fail because of the following reasons: 1) contact can not be represented efficiently from linear mode shapes; 2) nonlinear hyperfoam models, that possibly include visco-elasticity, are needed to represent the foam's hardening behavior; 3) very refined meshes would be required to capture the frequency content over 10,000 Hz. Although it may be possible to compute the solution via modal superposition for a single design, the multiplication of such operation in the context of inverse problem solving would be totally unfeasible.

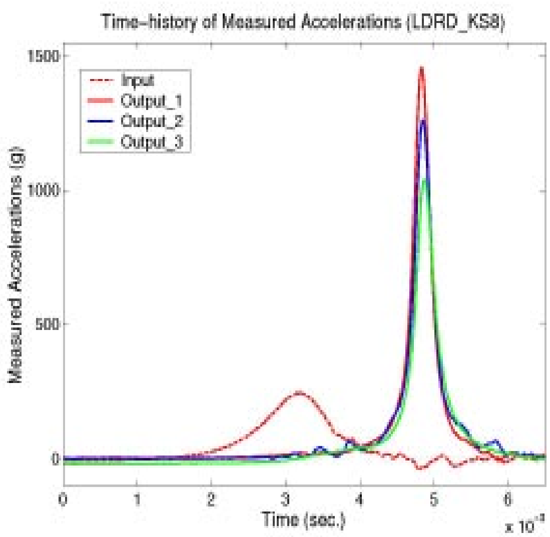

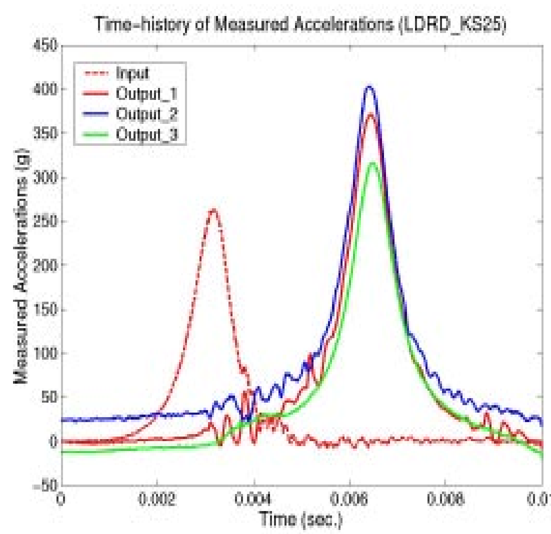

Figure 8. Input and output accelerations measured during a low-velocity impact.
(Left: impact on a thin layer of material. Right: impact on a thick layer of material.)

The results available are summarized in Table 2 that gives the number of data sets collected for each configuration tested. Dropping the carriage from two different heights results into different velocities at the time of impact. The values obtained by integrating the acceleration signal match the analytical formula $\dot{x}_{impact} = \sqrt{2gh_{drop}}$ and provide 60.4 in./sec. (1.5 m/sec.) and 222.9 in./sec. (5.7 m/sec.) for the low velocity and high velocity impacts, respectively. The reason why less data sets are available at high impact velocity is because these tests proved to be destructive to the elastomeric pad and could not be repeated to study the variability.

Table 2. Data collected with the impact testbed.

Number of Data Sets Collected	Low Velocity Impact (13 in./0.3 m Drop)	High Velocity Impact (155 in./4.0 m Drop)
Thin Layer (0.25 in./6.3 mm)	10 Tests	5 Tests
Thick Layer (0.50 in/12.6 mm)	10 Tests	5 Tests

We are also interested in validating an elastomeric material model for which test data are available. Since the original testing procedure that provided these data was quasi-static, it is our belief that the available model does not represent the actual behavior with good fidelity at high strain rates. Hence, combining the impact test (that provides sufficient resolution in the high strain region) to a numerical procedure for correlating time-domain measurements by optimizing the material's stress-strain curve defines a novel material testing procedure.

3. ASSESSMENT OF MODEL UPDATING TECHNIQUES

The first part of this research is overviewed in References [2-3] and it consists in attempting to formulate criteria for measuring the correlation between test data and finite element results for nonlinear vibrations. Since we have always constrained ourselves to 1) handle any type and source of nonlinearity and 2) enable both parametric and non-parametric updating to be carried out simultaneously, very few techniques have been found in the published literature that could meet our expectations. Typical examples of nonlinearities we are interested in include material nonlinearity, contact and impact at the interface between two components. These are typical of nonlinearity sources dealt with in the automotive and aerospace industries. As an illustration of this lack of techniques relevant to the nonlinear world, the reader is invited to review from References [6-7] the state-of-the-art in model updating technology. Among the earliest and most promising work in test-analysis correlation for nonlinear dynamics, we cite the work by Hasselman, Anderson and Wenshui [8] and the work by Dippery and Smith [9].

A short overview of the optimization framework usually implemented for adjusting parameters of a model is proposed in Section 3.1. Then, three examples are provided of techniques relevant to linear dynamics and modal data (Section 3.2). We focus on defining their metrics as a practical way to measure the distance between test and analysis data but details such as the computation of gradients, particular ways of resolving the spatial incompleteness and the numerical implementation are not addressed here. Results of applying these techniques to the LANL 8-DOF damage detection experiment are discussed in Section 3.3. In Section 3.4, a few metrics based on time series are proposed.

Finally, a demonstration of time-domain updating is provided in Section 3.5 using the LANL 8-DOF testbed. Two problems are illustrated: 1) identifying the location and extent of structural damage using time-domain data; and 2) identifying an internal force based on partial measurements.

3.1. THEORY

Generally, parametric optimization is achieved by minimizing a "distance" between test data and predictions of the numerical model, whether this distance is evaluated in the time or frequency domain. The optimization problem can be formulated as the minimization of the cost function shown in equation (3) where the first contribution represents the metric used for test-analysis correlation and the second serves the purpose of regularization

$$\min_{\{\delta p\}} \sum_{j=1\cdots N_{test}} \left\{R_j(p+\delta p)\right\}^* \left[S_{RR_j}\right]^{-1} \left\{R_j(p+\delta p)\right\} + \{\delta p\}^T \left[S_{pp}\right]^{-1} \{\delta p\} \qquad (3)$$

Constraints such as $p_{min} \le (p_e + \delta p_e) \le p_{max}$ are added to the formulation to eliminate filter out local minima that would not be acceptable from a physical standpoint. In the test discussed in Section 3.3 for example, the parameters of interest $\{p\}$ are the seven spring stiffnesses allowed to vary of +/-30% about their nominal value. Weighting matrices in equation (3) are generally kept constant and diagonal for computational efficiency. They can also be defined as covariance matrices which formulates a Bayesian correction procedure, as shown in Reference [3]. The only real difficulty is then to track the evolution of the covariance coefficients as parameters in the model are adjusted.

Obviously, many choices for the metric $\{R_j(p)\}$ are available, the simplest of all being the difference between test and analysis modal parameters. It is also known in the model updating community as the output error residue, see Reference [10], because quantities being compared are outputs as opposed to the excitation inputted to the system

$$\left\{R_j(p)\right\} = \begin{Bmatrix} \omega_1^{test} - \omega_1(p) \\ \vdots \\ \omega_j^{test} - \omega_j(p) \\ \phi_{11}^{test} - \phi_{11}(p) \\ \vdots \\ \phi_{ij}^{test} - \phi_{ij}(p) \end{Bmatrix} \qquad (4)$$

Formulations based on optimization problems may not be as efficient as other approaches, such as formulating the adjoint problem [11], but they offer some advantages besides constituting the overwhelming majority of inverse problem solving techniques. Among others, the formulation (3) is independent of the set of partial differential equations or numerical solver used, independent of the optimization solver and defined only by the choice of metric $\{R_j(p)\}$. Nevertheless, we will demonstrate in Section 4 that this formulation is fundamentally wrong.

3.2. LINEAR MODEL UPDATING STRATEGIES

In addition to using the output residue documented in many publications among which we cite Reference [10], the results summarized in Section 3.3 below involve the definition of the force and hybrid modal residues defined in References [12] and [13], respectively. The first one is referred to as a "force" vector because it estimates the out-of-balance forces obtained when the (erroneous) model fails to match the measured dynamics

$$\{R_j(p)\} = \left([K(p)] - \left(\omega_j^{test}\right)^2 [M(p)]\right)\{\phi_j^{test}\} \tag{5}$$

The second one is referred to as a "hybrid" vector and it can be explained, in a simplified version, as being the displacement field produced by applying the force vector (5) to the static system. It can be defined as

$$\{R_j(p)\} = \{\phi_j^{test}\} - \{\varphi_j\} \tag{6}$$

where vector $\{\varphi_j\}$ is obtained by solving the following static system

$$[K(p)]\{\varphi_j\} = \left(\omega_j^{test}\right)^2 [M(p)]\{\phi_j^{test}\} \tag{7}$$

The actual definition of the hybrid modal residue is more sophisticated, it can handle incomplete measurements as well as noisy data. Reference [13] offers a complete derivation and addresses some of the implementation concerns. Clearly, the residue vectors (5) and (6) are dual and both vanish when the finite element model reproduces the measured data with accuracy. The first metric offers the advantage of being very easy to compute and the second one features nice properties in terms of numerical conditioning. The important issue of incomplete measurement which may introduce a mismatch between sensor locations and degrees of freedom of the model is addressed in both References [12] and [13]. An alternative to dealing with the problem of spatial incompleteness is to apply model reduction and the three metrics (4-6) accommodate condensation techniques with no difficulty. We emphasize that our purpose is not to compare various figures of merit for their efficiency to identify sources of modeling error but rather to illustrate the danger of modal-based updating when the system is characterized by a source of nonlinearity not accounted for by the numerical model. Here, for example, friction in the LANL 8-DOF system is not represented. Although the linear model provides a good agreement with test data before and after parametric correction, the update fails to yield a positive identification of damage.

3.3. VALIDATION OF MODAL-BASED METRICS

To illustrate that modal parameters are unable to characterize nonlinear dynamics properly, the numerical model associated with the LANL 8-DOF system is refined using three different cost functions based on metrics (4-6). The objective of this test is to make the updated, linear model match the identified mode shapes and frequencies with a better degree of confidence than the one illustrated in Table 1. In doing so, the main modeling error (a 14% stiffness reduction located at the fifth spring) should be identified. Each time, the seven stiffness parameters are optimized based on modal parameters extracted from the acceleration data. Measurements are assumed to be available at locations 1, 4 and 7 only and the mismatch between the identified and numerical mode shapes is resolved using the modal expansion procedure relevant to each metric. To decouple the definition of test-analysis correlation metrics from algorithmic considerations, several optimization solvers are used to minimize the three cost functions. In this study, the order-0, Simplex algorithm, the order-1, conjugate gradient algorithm and the order-2, BFGS and Levenberg-Marquardt methods are implemented. These classical solvers are described in many publications and manuscripts among which we cite Reference [14].

A typical correlation after updating is illustrated in Table 3. It shows that the original frequency errors have been reduced to very small amounts and that the correlation of mode shape vectors has been improved. Based on such good correlation, most analysts would agree on the success of the updating procedure. However, the adjustment brought to each of the spring stiffness values in Figure 9 proves it impossible to identify the precise location and extent of structural damage. Worse, false positives (that is, stiffness reductions predicted at locations where no damage was originally introduced) are obtained. In the context of a practical engineering application, such false positives would result into a wrong diagnosis and/or erroneous stress predictions.

Table 3. Test-analysis correlation of the LANL 8-DOF testbed for nonlinear vibrations.
(The table shows the correlation between the damaged system without impact between the masses and the adjusted linear model.)

Mode Number	Identified Frequency	FE Model Frequency	Modal Assurance Criterion (MAC)	Frequency Error
1	22.3 Hz	22.4 Hz	99.9%	0.3%
2	43.9 Hz	44.2 Hz	99.9%	0.6%
3	64.8 Hz	65.9 Hz	98.2%	1.7%
4	85.9 Hz	85.1 Hz	97.2%	-0.9%
5	99.7 Hz	99.8 Hz	99.6%	-0.1%

The top half of Figure 9 illustrates the correction brought to each of the seven springs when the force residue metric (5) is implemented. Similarly, results of the hybrid residue metric (6-7) are shown on the bottom half of Figure 9. The correlation listed in Table 3 corresponds to metric (5) and similar trends are obtained with metric (6-7). The output error residue (4) fails to provide any meaningful model and these results are not commented further here.

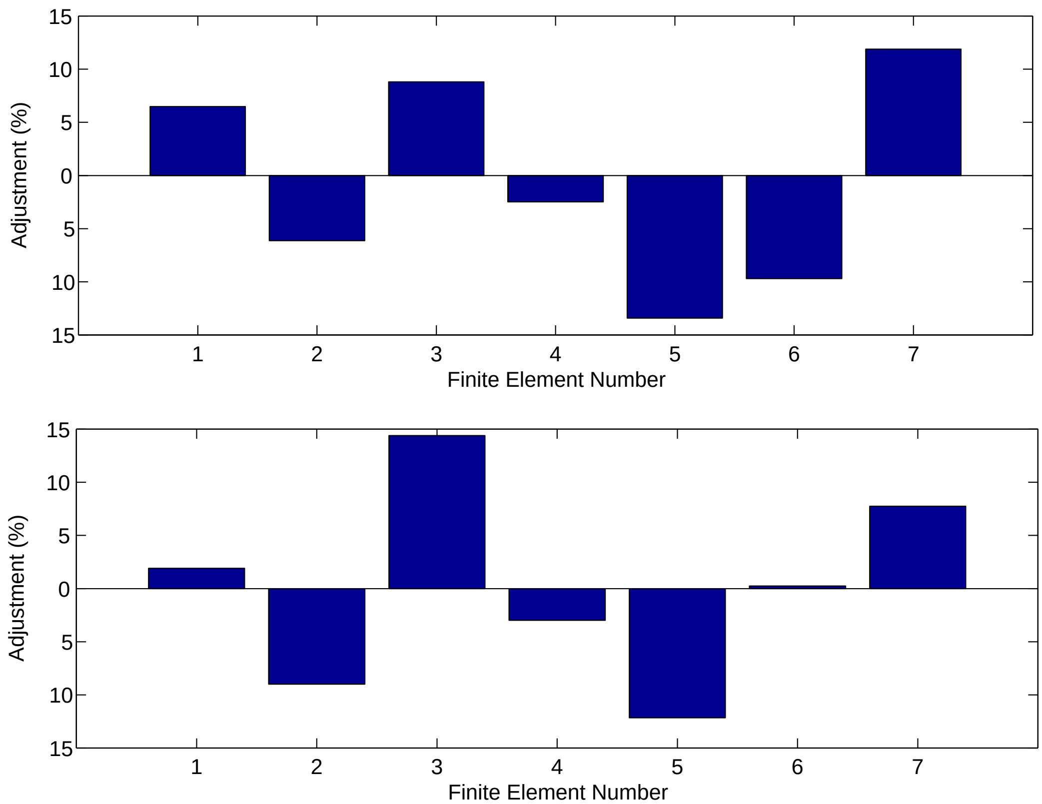

Figure 9. Adjustment (%) brought to the seven spring stiffness parameters.
(Top: force modal residues (5) are minimized. Bottom: hybrid modal residues (6-7) are minimized).

We conclude from these results that situations may arise where modal-based metrics fail to estimate the "true" correlation between two data sets when one of them or both represent a nonlinear system. In the example presented, the three metrics considered seem to indicate that various models match the test data when, in fact, the actual modeling error is not identified. Since various optimization solvers were implemented, we believe that these poor results are to blame on the metric itself and not on potential convergence difficulties. Our conclusion illustrates the need to define other metrics. Next, test-analysis correlation based on time series is discussed.

3.4. TIME-DOMAIN CORRELATION METRICS

Two time-domain metrics are introduced briefly. The first one correlates the measured and simulated signals directly while the second one correlates the subspaces to which these signals belong. This is achieved by making the numerical model match the singular values and vectors obtained by decomposition of the test data matrix, a procedure generally referred to as principal component decomposition (PCD). Reference [8] offers a complete description of this procedure. This presentation is not intended as an exhaustive discussion of time-domain metrics. Obviously, many choices are possible depending on the application targeted. Our purpose is to introduce a few basic correlation indicators and to test their efficiency using the testbeds defined in Section 2.

For clarity, we assume that the system of interest is modeled by a set of partial differential equations that can be integrated in time to provide the time-history of various state variables. In structural dynamics, the second-order equation of motion is described by

$$[M(p)]\left\{\frac{\partial^2 x(p,t)}{\partial t^2}\right\} + [K(p)]\{x(p,t)\} + \{F_{int}(p,t)\} = \{F_{ext}(t)\} \tag{8}$$

Equation (8) states that the system is in equilibrium when the applied loading in the right-hand side matches the combination of inertia and internal forces in the left-hand side. The nonlinear internal force vector $\{F_{int}(p,t)\}$ accounts for any nonlinear function of the system's state variables. Since the numerical model can be parametrized by a set of design variables $\{p\}$, time-domain responses such as the position vector $\{x(p,t)\}$ are shown to depend implicitly on these parameters. Next, we assume that time-varying quantities denoted by $\{u(t)\}$ are obtained from the state variables. These can represent arbitrary combinations of displacement, velocity and acceleration or any other quantity (strain, pressure, etc.) that may be needed for engineering analysis. In the example below, acceleration data are employed. Since our objective is to generate a more accurate model, the simplest and most natural metric is the root mean square (RMS) error between test and simulation data. The corresponding residue vectors are defined as

$$\{R(t)\} = \{u^{test}(t)\} - \{u(p;t)\} \tag{9}$$

The computational procedure consists of the following steps: 1) For a parametric model defined by a design $\{p\}$, the FE response is simulated via numerical integration of equation (8); 2) Residues (9) are calculated at prescribed degrees of freedom and time samples; and 3) The cost function $J(p)$ is optimized where

$$J(p) = \sum_{j=1\cdots N_t} \sum_{i=1\cdots N_s} \left(u_i^{test}(t_j) - u_i(p;t_j)\right)^2 + \alpha \sum_{k=1\cdots N_p} \left(p_k - p_k^{nominal}\right)^2 \tag{10}$$

For simplicity, equation (10) assumes a deterministic form. Nevertheless, generalization to a recursive Bayesian formulation offers no difficulty provided that the covariance matrices can be updated at low computational cost.

The PCD method validated in Reference [8] generalizes the notion of mode shape for nonlinear systems. Rather than using a direct comparison between time series, test and simulation data are first assembled into matrices

$$\left[U(t_i : t_f)\right] = \begin{bmatrix} u_1(t_i) & u_1(t_{i+1}) & \cdots & u_1(t_f) \\ u_2(t_i) & u_2(t_{i+1}) & \cdots & u_2(t_f) \\ \vdots & \vdots & \ddots & \vdots \\ u_{N_o}(t_i) & u_{N_o}(t_{i+1}) & \cdots & u_{N_o}(t_f) \end{bmatrix} \tag{11}$$

Then, the subspaces spanned by the rows (or columns) of such test and analysis, rectangular matrices are estimated using a singular value decomposition (SVD) expressed in terms of left, orthogonal singular vectors $\{\Phi_j\}$, right, orthogonal singular vectors $\{\Psi_j\}$ and singular values σ_j

$$\left[U^{test}\right] = \left[\Phi^{test}\right]\left[\Sigma^{test}\right]\left[\Psi^{test}\right]^T, \qquad \left[U(p)\right] = \left[\Phi(p)\right]\left[\Sigma(p)\right]\left[\Psi(p)\right]^T \tag{12}$$

Finally, the cost function used for optimizing the model's parameters $\{p\}$ is defined as a combination of the distance between the pseudo-subspaces (represented by the left singular vectors $\{\Phi_j\}$), the energy difference of each signal (represented by the singular values σ_j) and the error in time series (represented by the right singular vectors $\{\Psi_j\}$)

$$J(p) = \frac{1}{N_o^2}\left\|\delta\Phi(p)\right\|_2^2 + \frac{1}{N_o}\left\|\delta\Sigma(p)\right\|_2^2 + \frac{1}{N_o N_t}\left\|\delta\Psi(p)\right\|_2^2 + \alpha\left\|p - p^{nominal}\right\|_2^2 \tag{13}$$

where the normalized errors between test and analysis components of the SVD's are defined as

$$\begin{aligned} \left[\delta\Phi(p)\right] &= \left[\Phi^{test}\right]^T\left[\Phi(p)\right] - [I] \\ \left[\delta\Sigma(p)\right] &= \left[\Sigma^{test}\right]^{-1}\left(\left[\Sigma^{test}\right] - \left[\Sigma(p)\right]\right) \\ \left[\delta\Psi(p)\right] &= \left[\Psi^{test}\right]^T\left[\Psi(p)\right] - [I] \end{aligned} \tag{14}$$

Since the singular vectors are orthogonal, they provide a basis of the multi-dimensional manifold to which the nonlinear signals belong [15]. The PCD consists of minimizing the distance between these decompositions. In addition, the SVD offers a practical way of filtering out any measurement noise or rigid-body mode contribution because these are typically associated with singular values much smaller than those characteristic of the dynamics. However, we emphasize that the SVD can generally not be used for detecting the presence of a nonlinearity.

3.5. VALIDATION OF TIME-DOMAIN METRICS

The results are briefly discussed of applying the time-domain correlation metrics (RMS and PCD errors) to some of our testbeds. First, results with the 4-DOF numerical testbed are presented (Section 3.5.1). This illustration consists of reconstructing the evolution in time of design parameters when a set of incomplete, time-domain measurements are provided. Then, a numerical model is adjusted to locate structural damage in Section 3.5.2. The data set used originates from testing a linear configuration of the LANL 8-DOF system. Finally, Section 3.5.3 shows the identification of a time-varying internal force when a nonlinear version of this system is instrumented.

3.5.1. *Numerical Simulation*

One of the motivations for time-domain updating techniques is to identify the evolution in time of design parameters. This is for example critical to the area health monitoring where a system is instrumented continuously and the vibrating characteristics are analyzed to detect changes in its properties. Practically, multiple optimizations must be performed for successive time windows to “follow” the time-history of a subset of parameters, each parameter being assumed constant within a particular time window.

The example presented here illustrates this “successive optimizations” strategy. The 4-DOF system pictured in Figure 3 is optimized to identify a 15% stiffness reduction of its third spring using measurements at locations 1, 3 and 4. Since degree of freedom 2 is assumed to be unknown, model reduction is implemented to reduce the numerical model down to the subset of three measurements. Then, the reduced-order equation of motion is integrated in time and the RMS error (10) is optimized. Our reference solution is a noise-free simulation performed with the damaged set of parameters $\{k_1 = k_n; k_2 = k_n; k_3 = 0.85k_n; k_4 = k_n\}$ where k_n is the nominal stiffness equal to 322 psi (2.22 MPa).

Figure 10 represents the convergence obtained when the four stiffness parameters are optimized. Instead of performing a single optimization over the [0;0.2] sec. interval used for numerical integration, ten optimizations are performed over windows each 0.02 sec. in length. For this simple example, successive optimizations yield faster resolution times than a single optimization. The reason can be observed from Figure 10. The location and extent of damage are identified after a single optimization of 1/10-th the amount of data points; then, subsequent optimizations converge much faster because the starting point is very close to the optimum solution. Another explanation is that the time spent computing the cost function (10) or (13) is governed by the integration of the equation of motion. With smaller time windows, cost functions $J(p)$ are evaluated faster which also contributes to smaller computational times compared to the single optimization case.

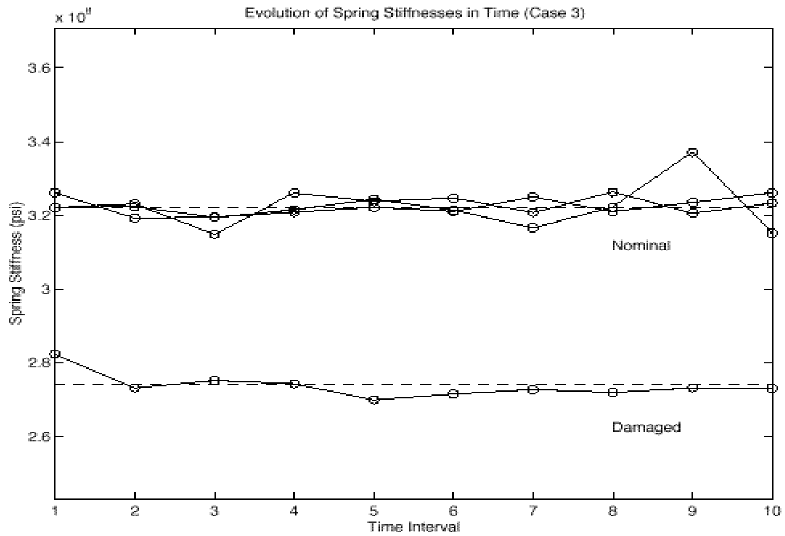

Figure 10. Convergence obtained during the optimization of four spring stiffness parameters. (The PCD cost function (13) is defined with measurements at locations 1, 3 and 4 on the 4-DOF testbed.)

We emphasize that, in this example, the nonlinear spring is known exactly and, therefore, the form of the model is available explicitly. The modeling error consists only of erroneous parameters which is the definition of a parametric optimization problem. This situation is different from the example discussed in Section 3.5.3 where the model form itself is incorrect which leads to non-parametric optimization.

3.5.2. *Detection of Structural Damage*

Next, results of applying the PCD cost function (13) to the LANL 8-DOF testbed are briefly summarized. The configuration used for this test is identical to the one described in Section 3.3 (same linear system, sensing configuration and damage scenario). The only difference is that, instead of using modal data to formulate the metrics, the PCD cost function is now implemented using three acceleration measurements over a single [0;2] sec. time window. Results discussed here can be compared directly with those of Section 3.3 (see Figure 9).

The adjustment brought to the seven springs is represented in Figure 11 in percentage of the original stiffness value. The only spring that witnesses a significant reduction is the fifth one, as expected. In addition, the 17% loss of stiffness predicted is in very good agreement with the 14% reduction inflicted during the vibration test. The stiffening of springs 1, 2 and 6 can not be explained other than by evoking the implicit least-squares nature of the solution procedure that tends to smear the adjustment throughout the set of parameters. Nevertheless, these corrections remain small in magnitude and inconsistent with a damage. As mentioned previously, we believe that friction plays an important role in the dynamics of the mass/spring system. The reason is that large modal damping ratios (over 10%) are identified from the test data which is inconsistent with the oscillations observed (the acceleration response does not feature an exponential damping anywhere comparable to 10%). The fact that friction is not accounted for in the numerical model may also contribute to the distortion of the solution.

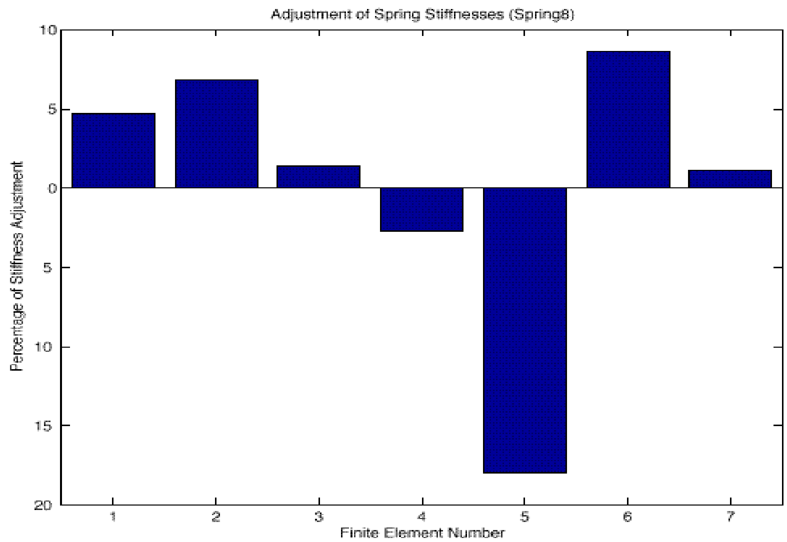

Figure 11. Adjustment brought to the seven spring stiffness values.
(Damage inflicted at spring 5 in the form of a 14% stiffness reduction is recovered by optimizing the PCD cost function defined with acceleration time-series at locations 1, 4 and 7.)

This example confirms our intuition that time-domain metrics may outperform modal-based metrics when the dynamics investigated is significantly nonlinear and/or modal parameters are not well suited to its description. They however introduce problems of their own that are addressed in Sections 4 and 5. Currently, this testbed is the object of further attention. Data sets featuring other damage scenarios and various severity of the nonlinearity are investigated with the help of more sophisticated numerical models. Our intent is to check whether this methodology always improves the predictive quality of our models.

3.5.3. *Identification of a Non-measured Internal Force*

The next test consists of applying the time-domain correlation technique to the identification of the internal, unmodeled force. In this example, a data set is used for which the contact mechanism is enabled, therefore, introducing a source of contact/impact during the vibrations. As before, only acceleration outputs at locations 1, 5 and 6 are assumed available. Since the correlation involves three measurements only, model reduction is implemented to condense the finite element matrices and force vectors. The particular technique chosen preserves exactly the lowest frequencies and mode shapes of the linear model [16]. Our model is perfectly linear except for the addition of an internal force vector. Arbitrary internal forces are applied at each one of the eight masses and test-analysis correlation is used for estimating these force levels at prescribed time samples.

The overall procedure goes as follows. Unknowns of the optimization are the eight force components. Correlation is based on the first 90 acceleration measurements that span a [0;0.168] sec. time window. For the numerical simulation, finite element matrices and force vectors are reduced to the size of the test model (locations 1, 5 and 6 only) and the response of the condensed model is integrated in time using 10 sampling points between any two measurements. As the response is integrated in time, the stiffness values and internal force vector are optimized. Figure 12 illustrates the correlation of the three acceleration outputs before and after the update when the cost function is defined by the PCD metric (13). Combining the reconstructed internal force to the linear model provides a clear improvement of its predictive quality.

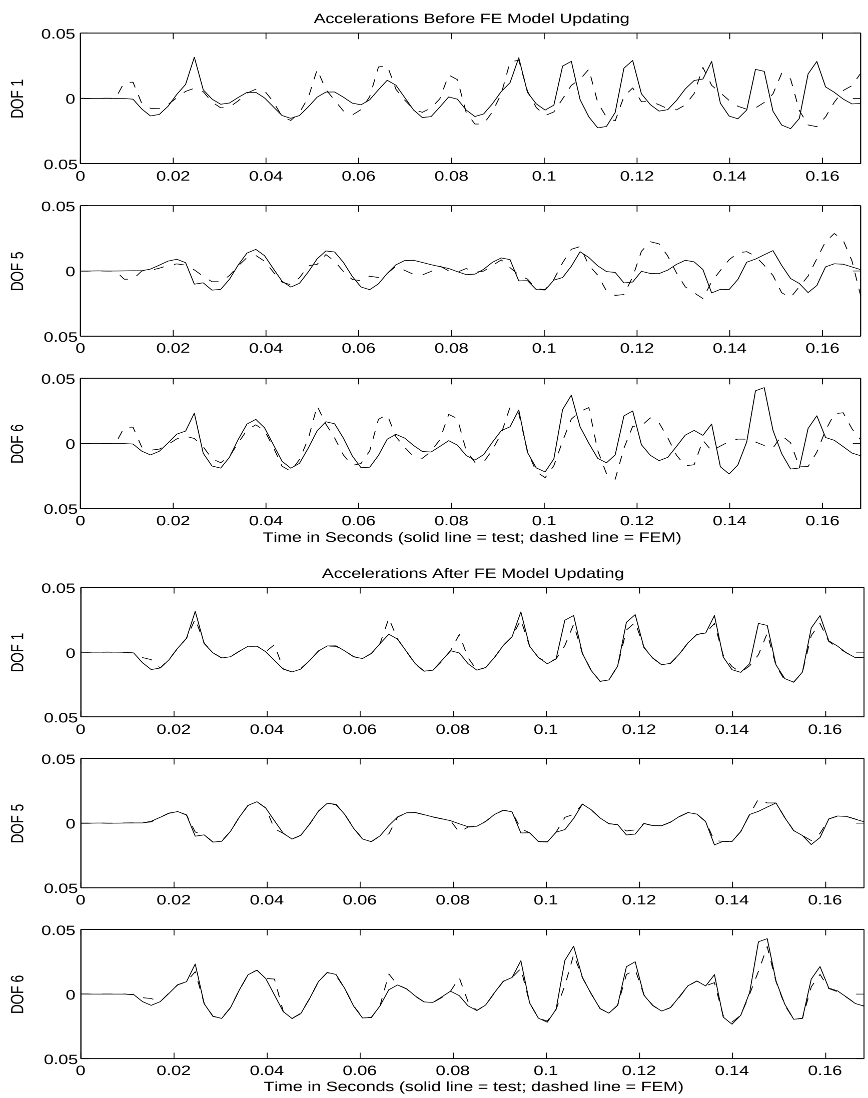

Figure 12. Comparison of measured and simulated acceleration time history for the LANL 8-DOF testbed. (Top: before non-parametric optimization. Bottom: after non-parametric optimization.)

Figure 13 shows the reconstruction of internal force as optimizations are performed for each time interval containing three consecutive measurements. In other words, 30 optimizations are performed, one every 0.0056 sec. No clear interpretation of this forcing function can be made. Notice however that the internal force at location 1 is approximately equal to zero which seems consistent with the fact that degree of freedom 1 is the driving point where the random excitation is applied.

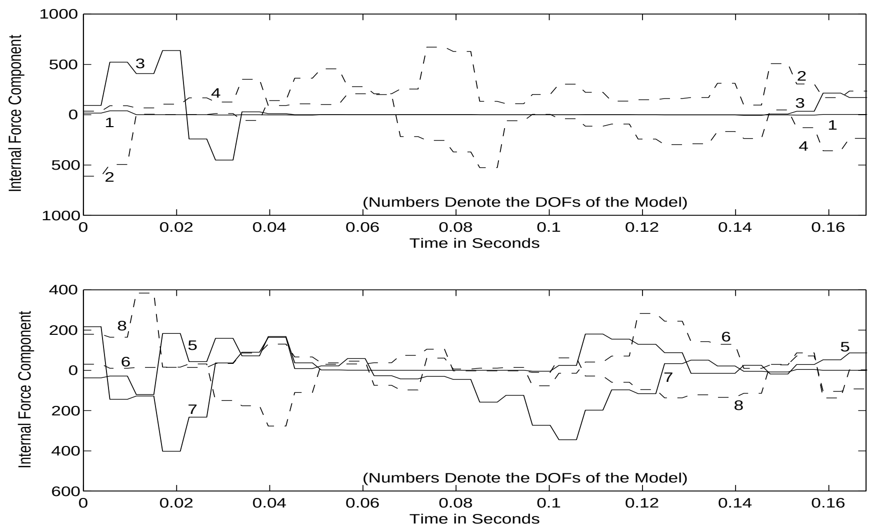

Figure 13. Time-history of the LANL 8-DOF system's internal forces obtained via model correlation.

This second application of the LANL 8-DOF testbed illustrates the concept of non-parametric updating via test-analysis reconciliation. Handling incomplete measurement sets seems to offer no significant difficulty other than computational but further investigation into this issue would be required before a definite conclusion can be reached. After having studied the case of nonlinear vibrations, the next step is to apply the time-domain techniques to transient test data. The impact testbed is developed for this purpose and future publications will demonstrate the validation of larger numerical models using test-analysis correlation in the context of explicit, time-domain solvers and probability integration (see the discussion in Section 5).

4. OPTIMAL ERROR CONTROL

One problem of time-domain model validation that has not been addressed previously is the reconstruction of continuous solution fields during the optimization. This issue is fundamental because, if the inverse problem is not formulated correctly, the numerical model yields discontinuous acceleration, velocity and displacement fields which contradicts the laws of mechanics for the class of problems investigated here. After explaining where discontinuous solution fields originate from, a new formulation of the inverse problem in the time domain is proposed. It is based on the theory of optimal control, as explained in References [9] and [17], and relies on the resolution of multiple two-point boundary value problems (BVP). When satisfactory solutions to the two-point BVP's are obtained, the numerical model is guaranteed to match the measured data at the beginning and at end of the time window considered. We emphasize that the idea of optimal error control is not an original one. Full credit must be given to the authors of References [9] and [17] although their motivation was somewhat different. Our contribution is to provide a complete derivation of the algorithm which is needed for the discussion in Section 4.5.

4.1. DISCONTINUITY OF THE SOLUTION FIELDS

The strategy of implementing successive optimizations produces several optimized models, one for each time window considered. This is necessary not only for computational purposes but also because some of the parameters being optimized may vary in time and following such evolution as it is occurring may be critical to model validation. However, nothing in the formulation of the inverse problem enforces continuity between the solution fields obtained from models optimized within the i-th and (i+1)-th time windows. Since the optimization variables can converge to different solutions $\{p^{(i)}\}$ and $\{p^{(i+1)}\}$ in two successive time windows, the discontinuity of the solution can be written, for example, in terms of the displacement field as

$$\lim_{\substack{t \to t_i \\ t \le t_i}} x(p^{(i)}, t) \neq \lim_{\substack{t \to t_i \\ t \ge t_i}} x(p^{(i+1)}, t) \qquad (15)$$

Of course, discontinuity arises only at the passage from one window to the next. This is artificial because the data record can be sub-divided into an arbitrary number of optimization windows. Figure 14 illustrates this problem for the previous 4-DOF example (see Section 3.5.1).

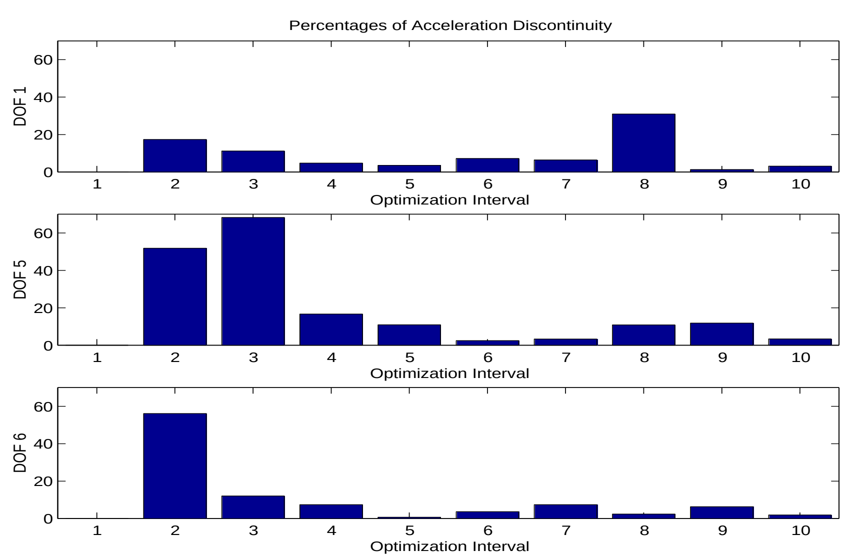

Figure 14. Discontinuity of the acceleration field (4-DOF testbed).

Figure 14 represents the average "jumps" obtained at locations 1, 3 and 4 as the acceleration values predicted at the end of the i-th time window are compared to values predicted at the beginning of the (i+1)-th time window for i=1...9. Although the design variables converge to the correct solution (see Figure 10), the sequence of models fails to provide continuous acceleration, velocity and displacement fields.

In the following, it is explained how optimal control strategies can be implemented to solve the inverse test-analysis correlation problem while reconstructing continuous solution fields and identifying the source of modeling error. An application to a single degree of freedom system shows that the optimal control approach does indeed resolve the discontinuity but also that practical applications remain out-of-reach because of the extreme computational requirement of the algorithm.

4.2. TEST-ANALYSIS CORRELATION VIA OPTIMAL ERROR CONTROL

For clarity, the evolution of the system investigated is recast as a set of first-order, partial differential equations. In structural dynamics, this would typically be achieved using the state-space form. We emphasize that the first-order formulation is used for simplicity only; the algorithm can be implemented in terms of second-order systems if computational efficiency dictates so, as we show in Section 4.3. Our starting point is a time-domain solver that provides a solution $\{x(t)\}$ to the set of nonlinear equations

$$\left\{\frac{\partial x}{\partial t}(t)\right\} = \{F(p,x,t)\} + \{e(t)\} \tag{16}$$

In equation (16), vector $\{e(t)\}$ represents the contribution of a generic modeling error. It includes everything that the numerical model does not account for. It is important to realize how general this definition is: the error contribution can be defined as a combination of modeling errors, discretization errors, etc., but it can also account for experimental or numerical variability. We also introduce the notation $\{y(t)\}$ that represents a vector of "features," that is, quantities obtained from the solution vectors $\{x(t)\}$ and that can also be assessed from the measurements. This vector can, for example, represent an arbitrary combination of acceleration and pressure data at various locations.

The inverse problem is re-formulated as follows. The objective is to reconstruct continuous, time series such as $\{x(t)\}$ in such a way that the features in $\{y(t)\}$ match the test data. Simultaneously, the procedure must provide a parametric adjustment of the model's design variables $\{p\}$ and identify the unknown, non-parametric error $\{e(t)\}$. For simplicity, the cost function is formulated as the RMS error between test and simulated data but it can be verified that any cost function may be used instead. Since the unmodeled dynamics plays a role identical to that of a controller in the theory of optimal control, a "minimum effort" penalty term must be added to avoid generating unrealistic error levels. Hence, the basic cost function can be stated as

$$J(p) = \sum_{k=1\cdots N_t} \left(\left\{ y^{test}(t_k) \right\} - \left\{ y(p,t_k) \right\} \right)^T \left[S_{yy}(t_k) \right]^{-1} \left(\left\{ y^{test}(t_k) \right\} - \left\{ y(p,t_k) \right\} \right) + \sum_{k=1\cdots N_t} \left\{ e(t_k) \right\}^T \left[S_{ee}(t_k) \right]^{-1} \left\{ e(t_k) \right\} \quad (17)$$

The resolution procedure is a direct application of the theory of optimal control. First, the cost function (17) is augmented with the evolution equation (16). This is achieved by introducing a vector $\{\lambda(t)\}$ of Lagrange multipliers (also referred to as the system's "co-state" variables) that penalize the total cost in the event where the state equation is not satisfied. The augmented cost function is defined as

$$\begin{aligned} \bar{J}(p;x;e) = & \sum_{k=1\cdots N_t} \left(\left\{ y^{test}(t_k) \right\} - \left\{ y(p,t_k) \right\} \right)^T \left[S_{yy}(t_k) \right]^{-1} \left(\left\{ y^{test}(t_k) \right\} - \left\{ y(p,t_k) \right\} \right) \\ & + \sum_{k=1\cdots N_t} \left\{ e(t_k) \right\}^T \left[S_{ee}(t_k) \right]^{-1} \left\{ e(t_k) \right\} - \left\{ \lambda(t_k) \right\}^T \left(\left\{ \frac{\partial x}{\partial t}(t_k) \right\} - \left\{ F(p;x;t_k) \right\} - \left\{ e(t_k) \right\} \right) \end{aligned} \quad (18)$$

Adding a set of variables $\{\lambda(t)\}$ may seem inconsistent with the objective of simplifying the resolution procedure. The reason is that these new unknowns provide additional equations that can be solved for to ensure that the numerical solution matches the test data at the beginning and at the end of each time window. The numerical algorithm is obtained in a classical manner by: 1) converting $\bar{J}$ into a continuous functional; 2) performing an integration over the time window $[t_i;t_{i+1}]$ considered; and 3) applying the necessary conditions $\frac{\partial \bar{J}}{\partial x} = 0$ and $\frac{\partial \bar{J}}{\partial e} = 0$. It yields the following set of governing equations that must be solved simultaneously in each time window $[t_i;t_{i+1}]$

$$\begin{aligned} & \left\{ \frac{\partial x}{\partial t}(t) \right\} = \left\{ F(p,x,t) \right\} + \left\{ e(t) \right\} \\ & \left\{ \frac{\partial \lambda}{\partial t}(t) \right\} = -\left[\frac{\partial F}{\partial x}(p;x;t) \right]^T \left\{ \lambda(t) \right\} \\ & \left\{ e(t) \right\} = -\frac{1}{2} \left[S_{ee}(t) \right] \left\{ \lambda(t) \right\} \\ & \left\{ \lambda(t_k^+) \right\} = \left\{ \lambda(t_k^-) \right\} + 2 \left[\frac{\partial y}{\partial x}(p,t_k) \right]^T \left[S_{yy}(t_k) \right]^{-1} \left(\left\{ y^{test}(t_k) \right\} - \left\{ y(p,t_k) \right\} \right) \\ & \left\{ x(t_i) \right\} = \left\{ x^{test}(t_i) \right\} \text{or} \left\{ \lambda(t_i^-) \right\} = 0 \\ & \left\{ x(t_{i+1}) \right\} = \left\{ x^{test}(t_{i+1}) \right\} \text{or} \left\{ \lambda(t_{i+1}^+) \right\} = 0 \end{aligned} \quad (19)$$

It can be observed that the fourth equation above represents the discontinuity of the co-states. As expected, it is shown to be a direct consequence of how well test data are reproduced by the numerical model. To the extent where the observation vector matches the test data exactly, no discontinuity is propagated to the co-states. The last two of equations (19) ensure that the test data are reproduced at the beginning and at the end of each time window. The only remaining step is to integrate this procedure to a parametric optimization solver. The solver itself may be any "black box" optimizer that the user finds convenient to implement. The basic requirement is that the value of a cost function $J(p)$ be obtained for any arbitrary design $\{p\}$. This calculation is summarized below.

4.3. NUMERICAL IMPLEMENTATION

To illustrate how the optimal control formulation can be applied to structural dynamics, equations are transformed back into their second-order form. The five-step procedure outlined below is encapsulated within the optimization solver. For a given set of variables $\{p\}$, the cost function $J(p)$ defined in equation (17) is calculated by:

Step 1. Choice of the initial condition $\{\lambda_o\}$: Given a particular design $\{p\}$, the co-state's initial condition must be obtained that minimizes the difference between test and numerical data. The cost function to minimize can, for example, be defined as the RMS error

$$J(\lambda_o) = \sum_{k=i,i+1} \left(\left\{ y^{test}(t_k) \right\} - \left\{ y(\lambda_o, t_k) \right\} \right)^T \left(\left\{ y^{test}(t_k) \right\} - \left\{ y(\lambda_o, t_k) \right\} \right) \tag{20}$$

This optimization problem introduces the two-point boundary value problem mentioned previously because, once the optimum is found, the observation vector is guaranteed to match test data at the time increments considered. The optimization problem defined by cost function (20) would typically be embedded into the outer, parametric optimization loop. In addition, calculating the feature vector $\{y(\lambda_o, t)\}$ for a given initial condition $\{\lambda_o\}$ requires the evaluation of Steps 2-5 below which renders the entire procedure extremely time-consuming.

Step 2. Time integration for the co-state: Once the initial condition has been optimized to ensure continuity of the solution fields, the co-state equation (19) is integrated. The equivalent second-order form is

$$[M(p)] \left\{ \frac{\partial^2 \lambda(t)}{\partial t^2} \right\} + [K(p)] \left\{ \frac{\partial \lambda(t)}{\partial t} \right\} = 0 \tag{21}$$

Note that this system is unstable: it can be verified that some of its eigenvalues are complex with a positive real part. Very short time windows $[t_i; t_{i+1}]$ must be considered so that oscillations do not have time to grow unstable. The obvious inconvenient is that shorter windows require more two-point BVP's to be solved.

Step 3. Reconstruction of the non-parametric, unmodeled dynamics:

$$\{e(t)\} = -\frac{1}{2}\left[S_{ee}(t)\right]\{\lambda(t)\} \tag{22}$$

Step 4. Integration of the equation of motion: The second-order equation of motion is integrated with the contribution of the modeling error identified at Step 3 and starting with the initial condition $\{x(t_i)\} = \{x^{test}(t_i)\}$ and $\{\dot{x}(t_i)\} = \{\dot{x}^{test}(t_i)\}$

$$[M(p)]\{\ddot{x}(t)\} + [K(p)]\{x(t)\} + \{F_{int}(p,t)\} = \{F_{ext}(t)\} + \{e(t)\} \tag{23}$$

Adding the error term in equation (23) guarantees that the displacement, velocity and acceleration fields match the measured data at the end of the current time window, $t_i = t_{i+1}$. Potential discontinuities are "absorbed" by the co-state and error variables. Note that the tolerance used for monitoring the convergence of the two-point BVP (20) defines the maximum allowed discontinuity of the solution fields. A trade-off between the continuity constraint and the computational requirement can therefore be achieved.

Step 5. Calculation of the cost function: Finally, the feature vector $\{y(t)\}$ is estimated using the solution fields obtained by integrating equation (23). The cost function $J(p)$ is calculated from one of the definitions (10) and (13) or any other if more appropriate metrics can be defined.

So far, the choice of matrices $\left[S_{yy}(t)\right]$, $\left[S_{ee}(t)\right]$ and $\left[S_{pp}(t)\right]$ (if a minimum-change contribution is added to the cost function) has not been discussed. If kept constant, it is most convenient to adopt diagonal matrices. However, Reference [9] reports that the selection of weights in $\left[S_{ee}(t)\right]$ can be critical to the overall convergence, in which case a second inner loop should be implemented to adjust these weights as needed. The weighting can also be defined in terms of covariance matrices for implementing a maximum likelihood approach or a Bayesian parameter identification method. Variance and covariance data in matrix $\left[S_{yy}(t)\right]$ are obtained directly from test data. Similarly, variance and covariance data in matrix $\left[S_{pp}(t)\right]$ are derived from the model's uncertainty characterization. The only computational difficulty is the evaluation and updating of the error covariance matrix $\left[S_{ee}(t)\right]$. The analyst must generally compromise between computational efficiency (that favors uncorrelated statistics and diagonal matrices) and accuracy (that requires higher-order approximations and multiple matrix factorizations).

To illustrate the optimal error control approach, a numerical example is presented that involves forced vibrations of the single-degree of freedom, Duffing oscillator. This simple, nonlinear system provides a good understanding of the method's capability and limitation, as discussed below.

4.4. NUMERICAL ILLUSTRATION USING A SINGLE DEGREE OF FREEDOM SYSTEM

To illustrate how the optimal control algorithm works for solving an inverse, test-analysis correlation problem, the Duffing oscillator presented in Section 2.1.1 is investigated.

As mentioned previously, the set of equations (1) is integrated in time to generate the reference data. Then, the internal force is removed. Therefore, the starting model is linear and the (unknown) modeling error is simply $e(t) = F_{int}(t)$. No noise is added although this would typically be handled by setting the covariance matrix $[S_{yy}(t)]$ to an upper-bound estimate of the amount of noise in each signal. Ten successive optimization windows $[t_i; t_{i+1}]$ are defined over the 30 sec.-time period and a total of 75 increments are used for integrating the solution within each window. The feature vector $\{y(t)\}$ considered simply collects the displacement and velocity responses at the eleven samples t_i where test data are assumed available. The error weighting matrix is kept constant with weights equal to one half

$$\left\{y^{test}(t_i)\right\} = \begin{Bmatrix} x^{test}(t_i) \\ \dot{x}^{test}(t_i) \end{Bmatrix}, \qquad \left\{y(p,t_i)\right\} = \begin{Bmatrix} x(p,t_i) \\ \dot{x}(p,t_i) \end{Bmatrix}, \qquad \left[S_{ee}(t_k)\right] = \begin{bmatrix} 0.5 & 0 \\ 0 & 0.5 \end{bmatrix} \tag{24}$$

Figure 15 illustrates the correlation of the updated model. The procedure outlined in Section 4.3 identifies the internal force as a function of time and this result is shown in Figure 16. It can be observed from Figure 15 that the optimized model is in perfect agreement with test data at the sampling points. The dashed line that represents the response of the model after optimization matches each measurement and provides a significant improvement over the original response in Figure 2. We emphasize that only points shown by the eleven stars in Figures 2 and 15 are used to fit the model; the baseline pictured by the solid line is shown only for the purpose of assessing whether or not the model reproduces the "continuous" solution. This example illustrates that the correlated model can generate continuous displacement, velocity and acceleration fields even though ten independent optimizations are performed.

It can be concluded from Figure 16 that the error identified from this procedure approaches the "true" cubic nonlinearity with a fair accuracy considering the small number of measurements used. Both the periodicity and overall amplitude of the nonlinear force are captured. At the very least, this solution would provide some insight into the nature of the nonlinearity and the approximate value of the nonlinear spring. For example, if a simple parametric model such as $e(t) = \alpha\left(x^3(t)\right)$ is curve-fitted in the least-squares sense to the values of $e(t)$ obtained in Figure 16, the nonlinear spring stiffness is estimated to be equal to $\alpha = 0.065$ instead of the value $k_{nl} = 0.05$ used (30% error).

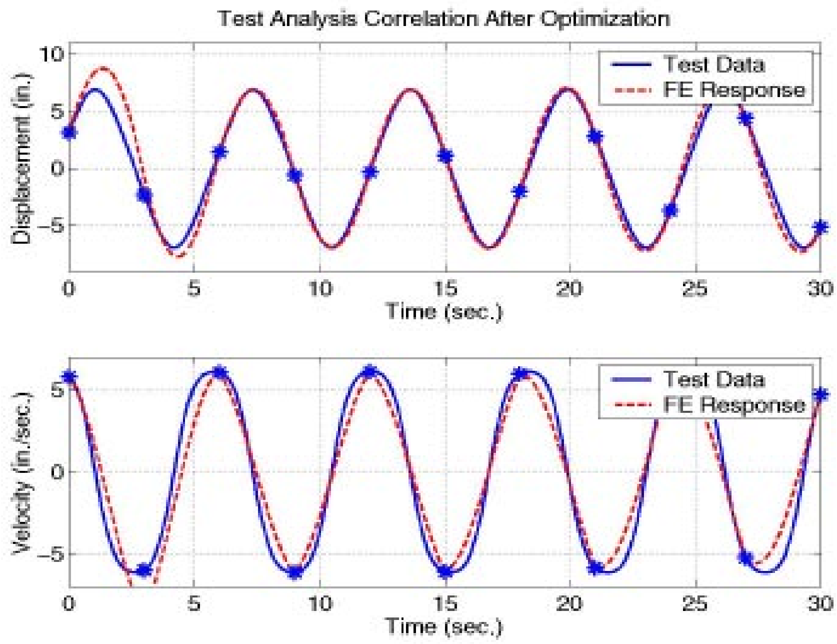

Figure 15. Test-analysis correlation of the single degree of freedom system after model updating. (Top half, displacement time-history; Bottom half, velocity time-history.)

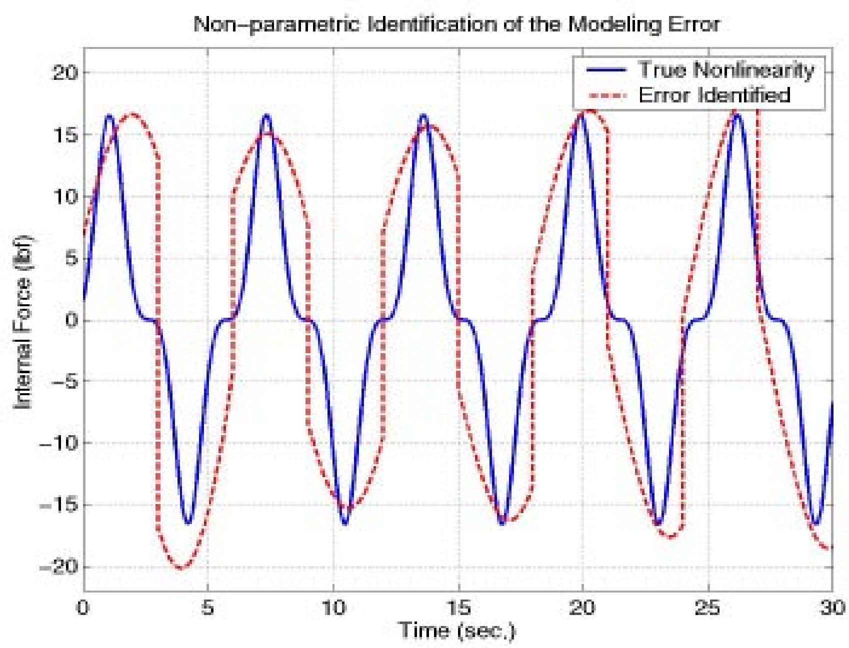

Figure 16. Non-parametric identification of the modeling error with the single degree of freedom system. (Test data are assumed to be available at 11 sampling points.)

Since the error vector is estimated directly from the co-states in equation (22), discontinuities obtained when the solution progresses from one time window to the next are visible in Figure 16. We emphasize that such discontinuities are artificial (because the number of time windows is arbitrarily chosen by the user) and a dedicated data treatment could be implemented to filter them out and curve-fit a continuous error field. The theory of optimal control states that the controller becomes continuous if an infinite number of observations are available. For our application, this means that the error vector should converge to the "true" error if more measurements are available.

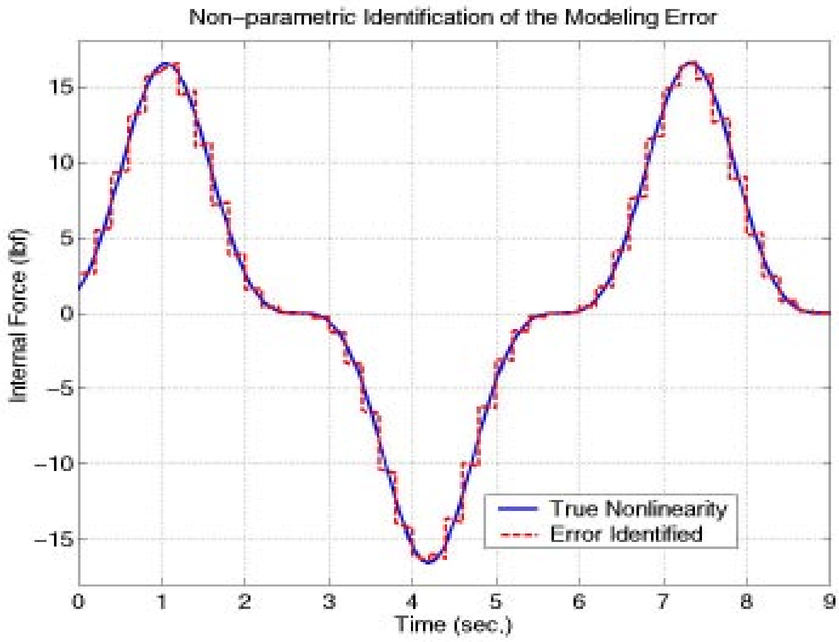

Figure 17. Non-parametric identification of the modeling error with the single degree of freedom system. (Test data are assumed available at 151 sampling points.)

This is verified in Figure 17. The same problem is analyzed with, this time, a total of 151 measurements. This results into 150 two-point BVP's and optimization problems. To keep the sampling period Δt unchanged, five increments are used for integrating the solution between any two successive measurement samples. In Figure 17, the true nonlinearity is represented by the solid line while the identified error is represented by the dashed line. It shows that the optimal error control delivers a very accurate estimation of the unknown dynamics as the number of measurements increases. A direct result is that the displacement, velocity and acceleration fields predicted by the optimized models, while remaining continuous, match the test data with even greater accuracy.

4.5. DISCUSSION OF THE RESULTS

The important conclusion that we emphasize in this Section is that extreme care must be brought to the formulation of model validation when time series are employed. Unconstrained optimization may result into discontinuous solution fields. This difficulty can be alleviated by formulating an optimal controller of the modeling error. This is a very attractive technique since not only does it handle parametric and non-parametric identifications simultaneously but it also propagates uncertainty and variability using the Bayesian theory of information and it provides a rigorous framework for generating continuous solutions from an arbitrary number of optimizations.

However, this improvement comes with the additional cost of formulating a two-point BVP to guaranty continuity of the solution. Since the procedure is embedded within an optimization solver, multiple two-point BVP's must be solved for. Unfortunately, the impact on the computational requirement is enormous. For example, solving the Duffing oscillator problem requires a total of 16 to 20 hours of CPU time depending on the number of measurement points available. The 4-degree of freedom system shown in Figure 3 is also investigated. This application consists in calculating the stiffness of each of the four springs and identifying the cubic internal force (assumed unknown). The resolution requires about 70 hours of CPU time. These timings are obtained on a dedicated R10,000/250 MHz processor when the algorithm is programmed within the environment provided by Matlab™.

Clearly, these figures prohibit any application of the technique to practical engineering problems. It is for this reason that other avenues must be explored. In the remainder, several key aspects of model updating for nonlinear systems are discussed and illustrated using real test data from our impact testbed.

5. DISCUSSION OF KEY ISSUES AND CHALLENGES

We wish to convince the reader that, for a wide variety of test-analysis applications, techniques based on linear dynamics and modal superposition are likely to fail. Hence, it is critical to validate numerical models by correlating transient test data rather than steady-state, modal data. However, formulating correctly the inverse problem in this case requires to solve multiple two-point boundary value problems, as explained in Reference [9] and illustrated in Section 4. Our preliminary investigation of these techniques indicates that their computational requirements prohibit their application to the types of problems we are interested in.

In addition to these difficulties, several problems have not yet been addressed. One of the most critical issue is the choice of data metrics. Using mode shapes and resonant frequencies provides an efficient filtering of "noise" and, in general, all random effects that may corrupt the underlying dynamics of the data set. When time-domain, nonlinear data are investigated, this must be achieved by the combination of statistical analysis and adequate test-analysis correlation metric. Among these important issues, we also cite the propagation of uncertainty through the analysis and the generalization to the multivariate case of statistics developed for measuring the consistency of a data point relative to a parent population. In the remainder, several issues are discussed that, we believe, are critical to the success of test-analysis correlation and model validation. They can be organized according to the following nine categories: 1) Characterizing the variability of an experiment/design; 2) Generating additional or surrogate data sets; 3) Extracting multiple features from the data; 4) Assessing statistically the consistency between multiple data sets; 5) Deriving high fidelity, physics-based material models; 6) Developing fast probability integration capabilities; 7) Calculating probabilistic sensitivity coefficients; 8) Generating fast running models; and 9) Developing strategies for model validation and verification. Our "philosophy" is to replace the formulation of inverse problems by a methodology where error surfaces are generated from the resolution of a large number of forward, stochastic analyses, then, optimized to identify the source of modeling error. We believe that this is the only alternative to the correct yet computationally impractical formulation discussed in Section 4. This procedure is summarized in Figure 18.

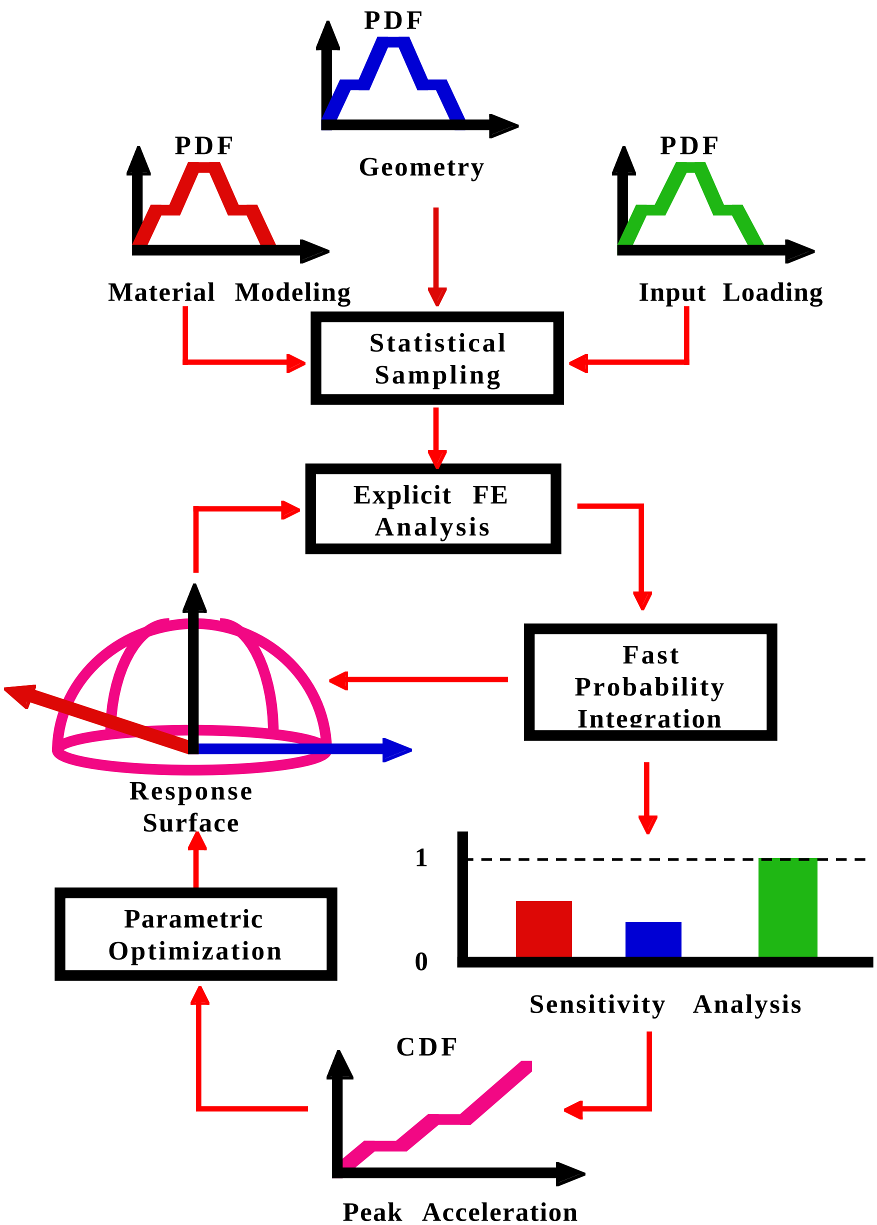

Figure 18. Flow chart showing the successive steps of model validation. (Arrows symbolize the flow of information.)

According to the procedure illustrated in Figure 18, optimization parameters and random variables are first defined. Multiple FE solutions and multi-dimensional error surfaces are generated from statistical sampling. Error surfaces provide a metric for test-analysis correlation and model updating. The first useful result is the sensitivity analysis used to reduce the subset of potential optimization variables down to the most sensitive ones. Then, the best possible model is sought through the optimization of its design parameters. Where these consist of random variables, the procedure must either search for the most likely parameters (case where distributions are known) or optimize the statistics (case where distributions are somewhat unknown). Finally, Figure 18 shows that, rather than comparing response levels, the ability of a probabilistic model to reproduce test data must be assessed using the response's cumulative density functions.

Besides having to account for uncertain inputs, imperfect material characterization and modeling errors during a design cycle, the other reason for this approach is to recast model updating as a problem of hypothesis testing. When the predictive quality of a model is assessed, we believe that three fundamental questions must be answered:

1) **Are results from the experiment(s) and simulation(s) consistent statistically?**
2) **What is the degree of confidence associated with the first answer?**
3) **If additional data sets are available, by how much does the confidence increase?**

Hypothesis testing permits to answer these questions. The difficulty however is to assess the minimum amount of data necessary to formulate a meaningful test and to implement such a test for large-scale, numerical simulations. Although hypothesis testing is well-known, very little literature is available on the subject of "population versus population" testing. Moreover, generalizing conventional tools to the multivariate case is not immediate. This makes the whole procedure a non-trivial task and a matter of open research to a great extent. In the remainder, the nine points listed previously are briefly addressed. Our purpose is not to review the corresponding state-of-the-art nor is it to provide an in-depth investigation into these issues. Instead, we motivate their importance and/or challenging aspects. Data from the LANL impact testbed are used to illustrate the discussion.

Variability of an Experiment or Design

Figure 19 shows the variability observed during the impact test (see Section 2.3) when the same configuration (same sample of elastomeric material and impact velocity) is tested ten times. In Figure 19, the top half represents the ten input acceleration signals measured and the bottom half shows the ten output acceleration signals measured at one of the three sensor locations. Although the environment of this experiment is very well controlled, a small spread in both input and output signals is obtained. This justifies our point that model correlation and validation must be formulated as statistical pattern recognition problems [18].

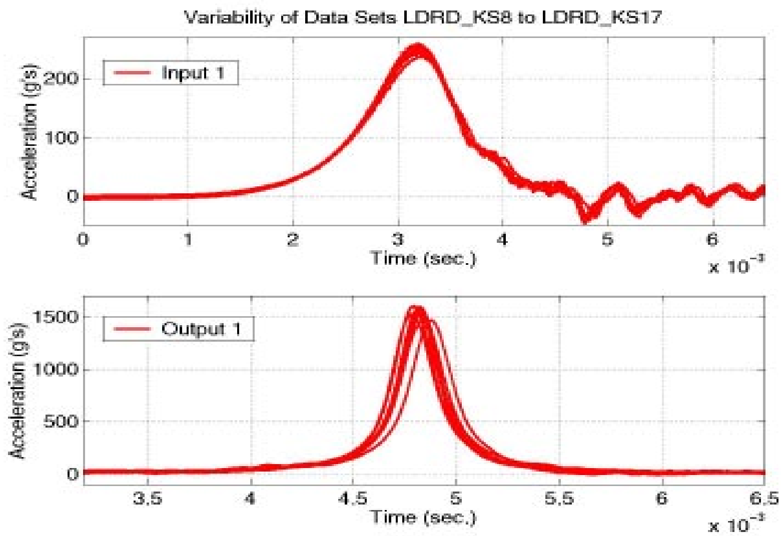

Figure 19. Acceleration signals measured during ten “similar” impact tests.

From Figure 19, variability of the test data can be assessed in a number of ways. The probability density function of the peak acceleration or that of the shock response function can be estimated if enough data sets are available. Such representation tells us, for example, that the most probable peak acceleration at output sensor 1 is equal to 1,520 g’s. What is therefore important is not necessarily that the correlated models reproduce the peak acceleration measured during a single test but that they predict the different acceleration levels with the same probability of occurrence as the one inferred from test data.

Additional or Surrogate Data Sets

This raises the question of the availability of multiple data seta. For many applications, the experiment can not be repeated and the amount of measurements available is insufficient to establish meaningful statistics. The method of surrogate data offers an attractive solution, as demonstrated recently in Reference [19] with an application to nonlinear dynamics. It can be used for generating additional data sets after the original distributions have been converted to unit Gaussian distributions via the Rosenblatt transform [20].

Similarly, it has been demonstrated that Monte Carlo simulations and the bootstrap are valid techniques for propagating external uncertainty sources. By this, we mean that additional data sets can be obtained even if a single experiment is available provided that the sources of uncertainty (sampling, A/D conversion, filtering errors; noise; etc.) can be reasonably estimated. By using these tools to investigate multiple data features rather than simple comparisons of time-series, we believe that a systematic procedure for the qualification of modeling uncertainty can be developed based on test-analysis correlation whether a single test or repeated experiments are available.

Feature Extraction

The next issue is therefore that of feature extraction. How can nonlinear, time-domain data be characterized if modal parameters are irrelevant? Application-dependent metrics that are often critical during the design can be defined but useful features must also provide a "fair" sensitivity with respect to input parameters and an overall measure of the agreement between test data and numerical simulations.

An illustration is provided using the PCD metric described by equations (11-12) and applied to one of the experimental data set collected during the impact test. Time measurements from the three sensors are gathered in data matrix (11) and its principal component decomposition (12) is calculated. The three singular values obtained from test data are equal to 8.79e+06, 0.85e+06 and 0.13e+06, which clearly indicates that the dynamics is dominated by a single "mode." Figure 20 pictures the three left singular vectors (or pseudo-mode shapes) and right singular vectors (or time series). Pseudo-mode shapes are normalized to unity and time series are scaled by the corresponding singular values. Although the measured acceleration responses are clearly dominated by a single "mode," the contribution from the second PCD vector is far from insignificant. It means that the dynamics of the impact is somewhat more complicated than first thought, probably due to the compression and stretching of the foam pad relative to the impactor. From the left singular vectors, it can be deducted that the first mode corresponds to the rigid-body steel impactor compressing the foam pad because the vector exhibits roughly the same amplitude at the three sensors. The second vector indicates that the impactor/foam assembly features a small inclination compared to the carriage. The last vector probably involves elastic deformations of the steel impactor (first bending mode).

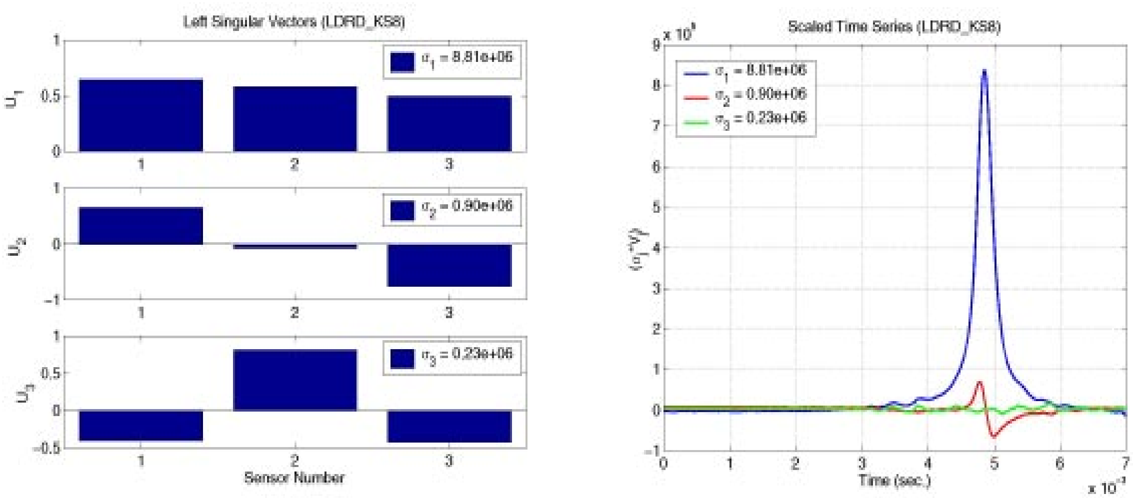

Figure 20. Principal component decomposition of the LANL impact test data.
(Left: pseudo-modes normalized to unity. Right: time series scaled by singular values.)

This example illustrates that important insight regarding the dynamics of the system can be gained from the analysis of adequate data metrics. Obviously, we would want for a validated, numerical model to reproduce these features and not just duplicate time-domain responses. The assessment of other metrics for test-analysis correlation is currently being investigated with the firm belief that advantage can be taken from their diversification. Handling various data features, however, introduces the problems of normalization and statistical assessment of multiple data sets and, possibly, multiple models. This last issue is addressed below.

Statistical Assessment of Multiple Data Sets

One of the open research issues that this work has identified is the problem of establishing a correlation between multiple data sets. By this we mean "assessing the degree to which two populations are consistent with each other." Our literature review seems to indicate that tools for assessing the distance between multiple data sets are not readily available in the context of statistical correlation and multivariate analysis.

This difficulty is illustrated in Figure 21. It represents the peak acceleration values for channels 1 and 2 plotted against each other. Data from repeated experiments and results from multiple simulations with two different models are shown. The three ellipsoids in Figure 21 illustrate the 95% confidence intervals. Obviously, the predictive quality of one of the two models is better because most of its data points (68 of 100) fall within the 95% confidence interval of the test data. The other model predicts only 34 of 100 points within the test's 95% confidence interval.

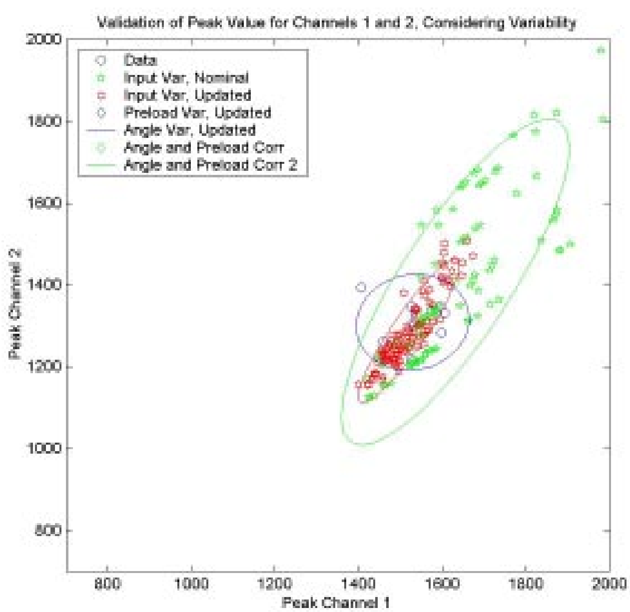

Figure 21. Comparison of test and analysis data in a two-feature space.
(The 2D space represents the peak accelerations measured or predicted at sensors 1 and 2.)

The investigation of multiple features against each other provides a powerful analysis tool. For example, the ability of the model to capture the sources of variability can be assessed from comparing the shape of confidence ellipsoids in Figure 21. Obviously, this assessment would be impossible with the analysis of time-histories. Unfortunately, quantitative indicators of the model's fit to test data are required when more than two features are involved because higher-order graphics are difficult to interpret visually. Although it remains an area of open research, a statistical test such as the Kolmogorov-Smirnov hypothesis test can measure the consistency between data points and cumulative density functions. In more complicated, multiple feature cases (see Figure 21), metrics such as the Kullback-Liebler relative entropy may characterize the consistency between statistics of the test and analysis populations. These two particular techniques are attractive because they are independent of the parent distribution which would be a necessary condition when the objective is precisely to characterize a population.

Fast Probability Integration for Large-scale Structural Dynamics

The notions discussed in this Section rely strongly on the capability to propagate variability throughout an analysis. For large-scale applications featuring nonlinear, explicit models composed of several million elements, Monte Carlo methods remain computationally too inefficient when it comes to predicting unlikely or catastrophic events, which is one of the main reasons for carrying out an analysis. Stochastic finite element techniques and fast probability integration methods must therefore be developed and interfaced with engineering codes.

This capability, that we are currently developing at Los Alamos National Laboratory through a module for reliability analysis called NESSUS [21], is illustrated in Figure 22. To validate our hyperfoam model, the peak acceleration observed during impact testing is predicted after having characterized the uncertainty of the simulation. The uncertainty is assessed by defining several random variables associated to the type of contact conditions implemented, the material modeling, the preload applied by tightening the center bolt and the velocity at time of impact. Fast probability integration propagates these distributions using a relatively small number of finite element solutions. Figure 22 represents the resulting probability distribution of the peak acceleration at output sensor 1. It can be seen, for example, that the probability that the peak acceleration be less than 1,520 g’s is equal to 90%. Based on this result, the consistency with test data (see Figure 19) can be established.

The feature’s probability density functions can also be differentiated with respect to each one of the random variables. This information is used for selecting the most sensitive parameters in a manner similar to an analysis performed with a deterministic model. Due to the nature of random variables however, we emphasize that derivatives can not be estimated with respect to the variables themselves. Instead, their statistics are employed which seems to provide satisfactory results in most cases. Sensitivity analysis for stochastic models is another area that currently generates a lot of theoretical and applied research.

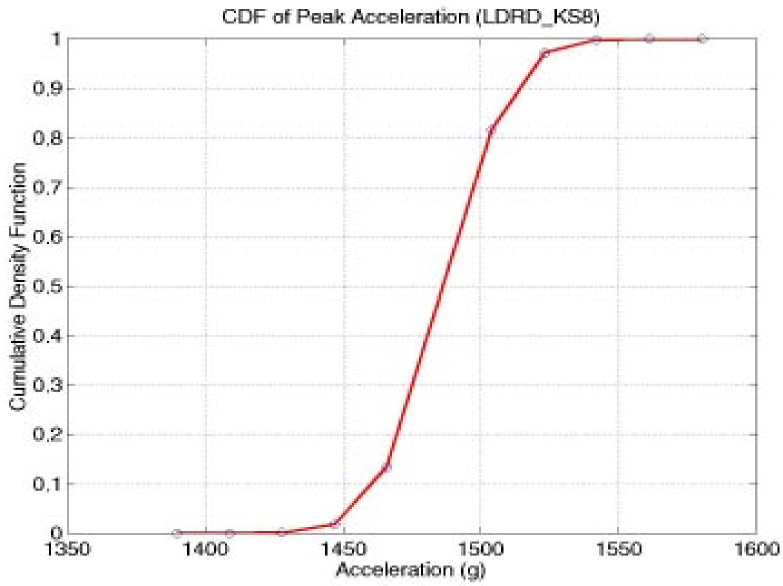

Figure 22. Cumulative density function of the peak acceleration.

Fast Running Models

If the correlation with test data is not satisfactory, the next step is to update a subset of the model's design variables with the objective of improving its predictive quality with respect to the features selected. Efficient numerical optimization requires that the objective functions and their gradients be obtained at low computational cost. Therefore, fast running models must be generated to replace the expensive, large-scale simulation.

This concept is illustrated in Figure 23 for the impact test. The two horizontal axes represent values spanned by an angle of impact and a scaling coefficient for the hyperfoam model. The vertical, log-scaled axis represents the PCD cost function (13) obtained by comparing the model's three output accelerations to test data. A total of 9 by 9 designs are analyzed to produce this error surface. These models are independent from each other and they would typically be analyzed in parallel. An equivalent, fast running model may be obtained by fitting a polynomial through the 81 data points available. A quadratic surface would, for example, be represented by

$$J(p_1;p_2) = \alpha_0 + \alpha_1 p_1 + \alpha_2 p_2 + \alpha_3 p_1 p_3 + \alpha_4 p_1^2 + \alpha_5 p_2^2 \tag{25}$$

and the six unknown coefficients $(\alpha_0;\alpha_1;\cdots;\alpha_5)$ would be best-fitted to the data in a least-squares sense. The agreement of a particular design with test data can then be interpolated everywhere within the region spanned by the input parameters and without having to run the full computation. It is also reported in the recent literature that neural networks have been applied to this problem with great success.

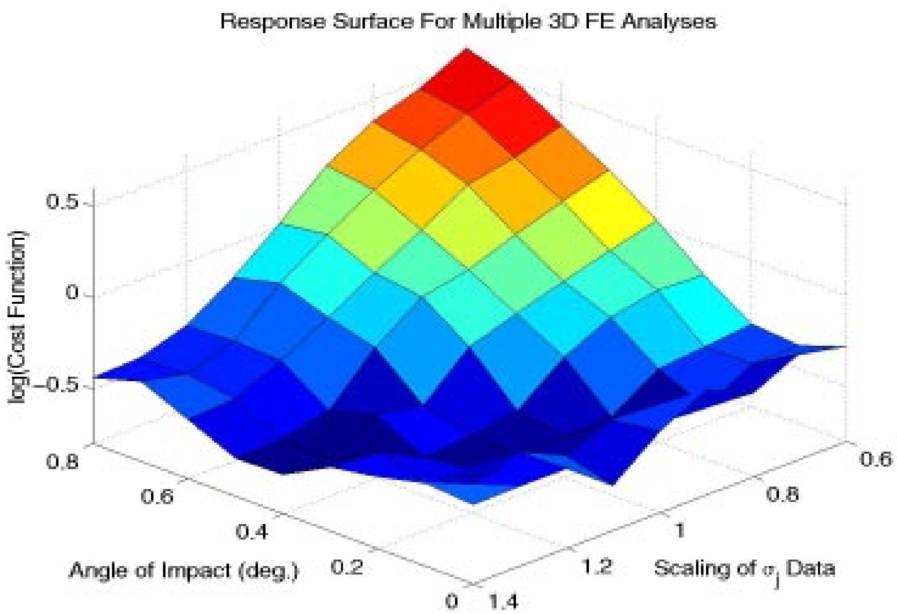

Figure 22. Error surface defined from the PCD of test data and simulation results.

Two issues relative to the generation of error surfaces are now briefly discussed. First, the problem of selecting the design points where the system's response is obtained must be addressed. This is important especially when the experiment or numerical simulation is time and resource consuming. If the input parameters are random variables, the uniform sampling pictured in Figure 22 may not provide enough information in regions where the feature's joint probability density function is maximum. This leads to a waste of computational time in the best case and to inconclusive results in the worst case. Statistical tests must be used to select the next experiment to be run or the next model to be analyzed with the objective of providing the best possible understanding of the output given a set of stochastic inputs. This particular area is the focus of recent advances in the statistics community [22].

Secondly, error surfaces must represent the stochastic nature of the problem when the objective is to account for sources of variability in the experiment and numerical model. For example, the deterministic metric pictured in Figure 22 may become a joint probability density function or a statistical, "goodness-of-fit" indicator used for formulating a hypothesis test. As before, the data available can be synthesized into a fast running model

$$J(p_1;p_2) = \alpha_0 + \alpha_1 p_1 + \alpha_2 p_2 + \alpha_3 p_1 p_3 + \alpha_4 p_1^2 + \alpha_5 p_2^2 + n(p_1;p_2) \tag{26}$$

with the main difference that the stochastic nature of the information manipulated must be recognized. This is achieved in equation (26) by adding a stochastic process $n(p_1;p_2)$ that would typically be best-fitted to the data to represent the characteristics of its distribution. Stochastic processes can also be included to propagate other sources of discrepancy between test and analysis data such as numerical and truncation errors or to bound the total uncertainty of the experiment. At this point, the idea of fast running, stochastic models requires more investigation but it seems very promising for bridging the gap between "parameter uncertainty" (that is, the approach that consists in parametrizing all modeling errors and sources of uncertainty) and "global uncertainty" (that is, the approach that consists in capturing the structure of the error without necessarily attempting to identify its source).

Strategies for Model Validation and Verification

The final step of a validation procedure is to verify that predictions of the optimized models are correct. This task is difficult because, in general, no additional data sets are available for the verification. In the conventional model updating literature, a model is thought to be validated when it matches the identified mode shapes and frequencies. However, this does not necessarily imply that the dynamics of a phenomenon has been captured correctly because modal parameters span a subspace of the actual response. With nonlinear dynamics, things get worst because the notion of subspace breaks down. This is the old mathematical dilemma between interpolation and extrapolation. Our "philosophical" view of this issue is that model validation does not exist. There is only model "invalidation" as demonstrated by Pearson's work on hypothesis testing [23], that is, a model may be considered correct as long as it can not be proved wrong. Practically, this means that: 1) Data sets not used during the validation step are required to assess the predictive quality of a model; and 2) Probabilities must be assigned to each model developed to reflect the degree of confidence (or lack of confidence) in their predictions. This approach is illustrated in Figure 23 with the impact testbed for which two configurations are validated independently of each other.

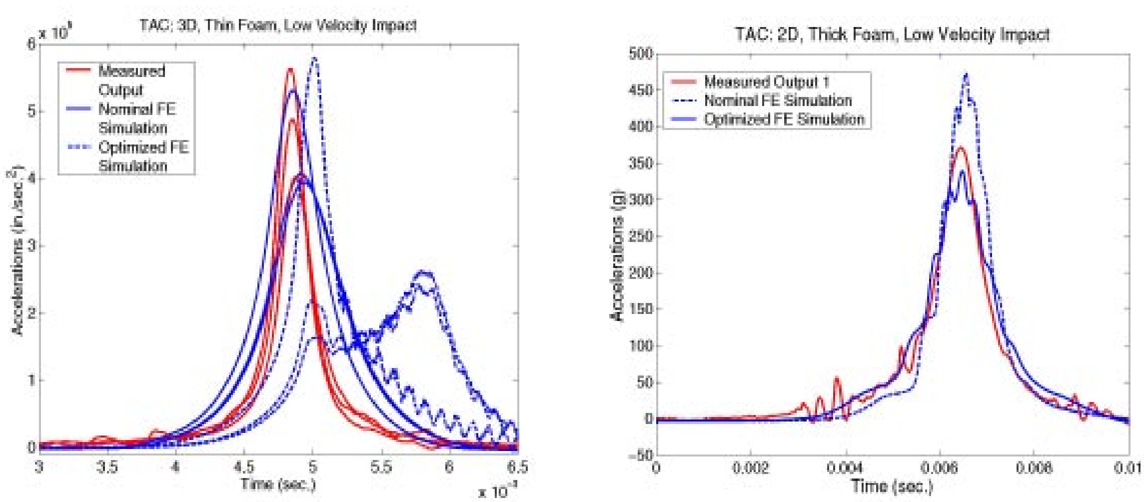

Figure 23. Verification of the model's prediction with test data not used during the optimization.

In this example, a 3D model featuring the thin foam pad (0.25 in.) is optimized to match the measured data. The optimization provides a set of optimal values for the hyperfoam model, the bolt preload and the angle of impact. Correlation of the original and final 3D models is shown on the left of Figure 23. The response of the nominal model at the three output locations is shown in dashed line while the same response is shown in solid line for the optimized model and instrumented system. Despite small oscillations attributed to numerical noise generated by the contact algorithm, the optimized model predicts the acceleration levels measured during the test. Note that the metric used for refining the numerical model (PCD) differs from the metric used to assess the correlation with test data which, we believe, provides additional confidence in the final result. Then, the optimal material model and the bolt preload are combined with a thick foam pad (0.50 in.) to validate the predictions of an axi-symmetric model. We emphasize that, during this second, independent step, a different configuration of the system, a different data set and a different numerical model are used. Correlation of the original and final 2D models is shown on the right of Figure 23. Once again, a clear improvement of the model's prediction is witnessed.

6. CONCLUSION

The work presented in this publication addresses the correlation of nonlinear models with test data. One of the specificity is that modal superposition can generally not be considered as a valuable solution technique due to its inability to represent arbitrary nonlinearity and to capture the dynamics of transient events. For this reason, test-analysis correlation must rely on time series. Several testbeds developed at Los Alamos National Laboratory in support of our health monitoring and code validation and verification programs are presented. Their purpose is to provide experimental data for validating the strategies implemented for test-analysis correlation and inverse problem solving. Linear model updating techniques are reviewed and their inefficiency is illustrated using a testbed developed to analyze nonlinear vibrations. Then, time-domain techniques are discussed and applied with greater success. Finally, we demonstrate that a careless formulation of the inverse problem in the time domain yields discontinuous solution fields which violates the most basic laws of mechanics. This difficulty is alleviated by formulating an optimal controller of the modeling error. This technique is capable of simultaneously 1) handling parametric and non-parametric identifications; 2) propagating uncertainty and variability using the Bayesian theory of information; and 3) providing a rigorous framework to generate continuous solutions from an arbitrary number of optimizations. Its computational requirement however makes it impractical for solving meaningful engineering problems.

To bypass some of the difficulties identified in this work, our current emphasis is on replacing inverse problems with multiple forward, stochastic problems. After a metric has been defined for comparing test and analysis data, response surfaces are generated that can be used for 1) assessing in a probabilistic sense the quality of a particular simulation with respect to "reference" or test data; and 2) optimizing the model's design parameters to improve its predictive quality. One critical issue to be investigated in future research is the definition of adequate metrics for correlating transient, nonlinear data. Rather than attempting to define deterministic distances, future work will emphasize dealing with “clusters” of test and analysis data that must be compared in a statistical sense.

REFERENCES

1. Lieven, N.A.J., and Ewins, D.J., “A Proposal For Standard Notation and Terminology in Modal Analysis,” *10th SEM International Modal Analysis Conference,* San Diego, California, Feb. 2-5, 1992, pp. 1414-1419.

2. Hemez, F.M., and Doebling, S.W., “Test-Analysis Correlation and Finite Element Model Updating for Nonlinear, Transient Dynamics," *17th SEM International Modal Analysis Conference,* Kissimmee, Florida, Feb. 8-11, 1999, pp. 1501-1510.

3. Hemez, F.M., and Doebling, S.W., “A Validation of Bayesian Finite Element Model Updating for Linear Dynamics," *17th SEM International Modal Analysis Conference,* Kissimmee, Florida, Feb. 8-11, 1999, pp. 1545-1555.

4. Beardsley, P., Hemez, F.M., and Doebling, S.W., “Updating Nonlinear Finite Element Models in the Time Domain,” *Structural Monitoring 2000,* F.-K. Chang (Ed.), *2nd International Workshop on Structural Health Monitoring,* Stanford University, Stanford, California, Sep. 8-10, 1999, pp. 774-783.

5. **Abaqus/Explicit**, User’s Manual, Version 5.8, Hibbitt, Karlsson & Sorensen, Inc., Pawtucket, Rhode Island, 1998.

6. Imregun, M., and Visser, W.J., “A Review of Model Updating Techniques,” *Shock and Vibration Digest*, Vol. 23, No. 1, 1991, pp. 19-20.

7. Mottershead, J.E., and Friswell, M.I., “Model Updating in Structural Dynamics: A Survey,” *Journal of Sound and Vibration*, Vol. 162, No. 2, 1993, pp. 347-375.

8. Hasselman, T.K., Anderson, M.C., and Wenshui, G., “Principal Components Analysis For Nonlinear Model Correlation, Updating and Uncertainty Evaluation,” *16th SEM International Modal Analysis Conference,* Santa Barbara, California, Feb. 2-5, 1998, pp. 664-651.

9. Dippery, K.D., and Smith, S.W., "An Optimal Control Approach to Nonlinear System Identification," *16th SEM International Modal Analysis Conference,* Santa Barbara, California, Feb. 2-5, 1998, pp. 637-643.

10. Piranda, J., Lallement, G., and Cogan, S., "Parametric Correction of Finite Element Models By Minimization of an Output Residual: Improvement of the Sensitivity Method," *9th SEM International Modal Analysis Conference*, Firenze, Italy, Jan. 1991.

11. Hanson, K.M., Cunningham, G.S., and Saquib, S.S., "Inversion Based on Computational Simulations," Maximum Entropy and Bayesian Methods, Erickson, G.J., Rychert, J.T., and Smith, C.R., Editors, Kluwer Academic, Dordrecht, Germany, 1998, pp. 121-135.

12. Hemez, F.M., and Farhat, C., "Structural Damage Detection Via a Finite Element Model Updating Methodology," *SEM International Journal of Analytical and Experimental Modal Analysis*, Vol. 10, No. 3, July 1995, pp. 152-166.

13. Chouaki, A.T., Ladevèze, P., and Proslier, L., "Updating Structural Dynamics Models With Emphasis on the Damping Properties," *AIAA Journal*, Vol. 36, No. 6, June 1998, pp. 1094-1099.

14. Jacobs, D.A.H., **The State of the Art in Numerical Analysis**, Ed., Academic Press, London, U.K., 1977.

15. Mees, A.I., Rapp, P.E., and Jennings, L.S., "Singular Value Decomposition and Embedding Dimension," *Physical Review A*, Vol. 36, No. 1, July 1987, pp. 340-346.

16. Burton, T.D., and Young, M.E., "Model Reduction and Nonlinear Normal Modes in Structural Mechanics," *ASME AMD*, Vol. 192, 1994, pp. 9-16.

17. Mook, D.J, "Estimation and Identification of Nonlinear Dynamic Systems," *AIAA Journal*, Vol. 27, No. 7, July 1989, pp. 968-974.

18. Bishop, C.M., **Neural Networks for Pattern Recognition**, Clarendon Press, Oxford University Press, Inc., New York, New York, 1998.

19. Paez, T., Hunter, N., and Red-Horse, J., "Statistical Tests of System Linearity Based on the Method of Surrogate Data," *17th SEM International Modal Analysis Conference*, Kissimmee, Florida, Feb. 8-11, 1999, pp. 1495-1500.

20. Rosenblatt, M., “Remarks on a Multivariate Transformation,” *The Annals of Mathematical Statistics*, Vol. 23, No. 3, 1952, pp. 470-472.

21. **NESSUS**, User’s Manual, Version 2.3, Southwest Research Institute, San Antonio, Texas, 1996.

22. McKay, M., “Sampling Variability of Measures of Input-Variable Importance in Computer Models,” *3rd DoE/MICS Workshop on the Predictability of Complex Phenomena*, Los Alamos, New Mexico, Dec. 6-8, 1999.

23. Neyman, J., and Pearson, E.S., “On the Problem of the Most Efficient Tests of Statistical Hypotheses,” *Philosophical Transactions of the Royal Society*, Series A, Vol. 231, 1933, pp. 289-337.